

Land Cover Change Detection Techniques

Very-high-resolution optical images: A review

ZHIYONG LV, TONGFEI LIU, JÓN ATLI BENEDIKTSSON, AND NICOLA FALCO

Land cover change detection (LCCD) with remote sensing images is an important application of Earth observation data because it provides insights into environmental health, global warming, and city management. In particular, very-high-resolution (VHR) remote sensing images can capture details of a ground object and offer an opportunity to detect land cover changes in detail.

However, VHR images usually have high spatial resolution but contain limited spectral information. Therefore, LCCD with VHR optimal images performs poorly because of high intraclass variation and low interclass variance. In the past decades, various approaches have been promoted to smoothen noise, reduce pseudochanges, and preserve the details of detection maps with VHR images.

In this article, we first present an overview of the main issues in terms of algorithms, applications, and referred characteristics to promote a comprehensive and general understanding of the development of LCCD with VHR remote sensing images. Several key methodologies are compared with three pairs of real VHR optimal images. Finally, we discuss future challenges and opportunities in applying VHR remote sensing images in LCCD.

VHR IMAGE

Numerous remote sensing platforms, such as QuickBird, GeoEye, Worldview, and unmanned aerial vehicles (UAVs),

can capture ground details with VHR, given the considerable progress in remote sensing technology [1]. Despite the lack of definition of *VHR* in the literature, *VHR* usually refers to the resolution range from submeter to several meters [1]–[5]. These images can depict additional ground details in practical applications, such as the edge, shape, and texture of ground targets.

However, many studies have demonstrated that high resolution does not automatically mean high detection accuracy in practical applications because of the following reasons:

- ▶ VHR images usually have a higher intraclass variation than low- or medium-resolution images, resulting in decreased separability between different entities, such as roads and buildings [5]–[7].
- ▶ With respect to spatial resolution, the size of each pixel is smaller in a VHR image than in a low–medium-resolution image, and pixels are connected tightly to each other in a VHR image.

Therefore, when detecting changes and measuring their magnitude between a pair of bitemporal VHR images, salt-and-pepper noise is often used in the detection map [8]–[10].

Figure 1 shows the characteristics of a pair of VHR images for LCCD. As seen in the images, spectral variation in the changed and unchanged areas is large, indicating the low homogeneity for VHR images. This implies that it is very difficult to accurately measure consistently the changed magnitude for either unchanged or changed areas between a pair of bitemporal VHR images. Moreover, determining a binarization

Digital Object Identifier 10.1109/MGRS.2021.3088865
Date of current version: 8 July 2021

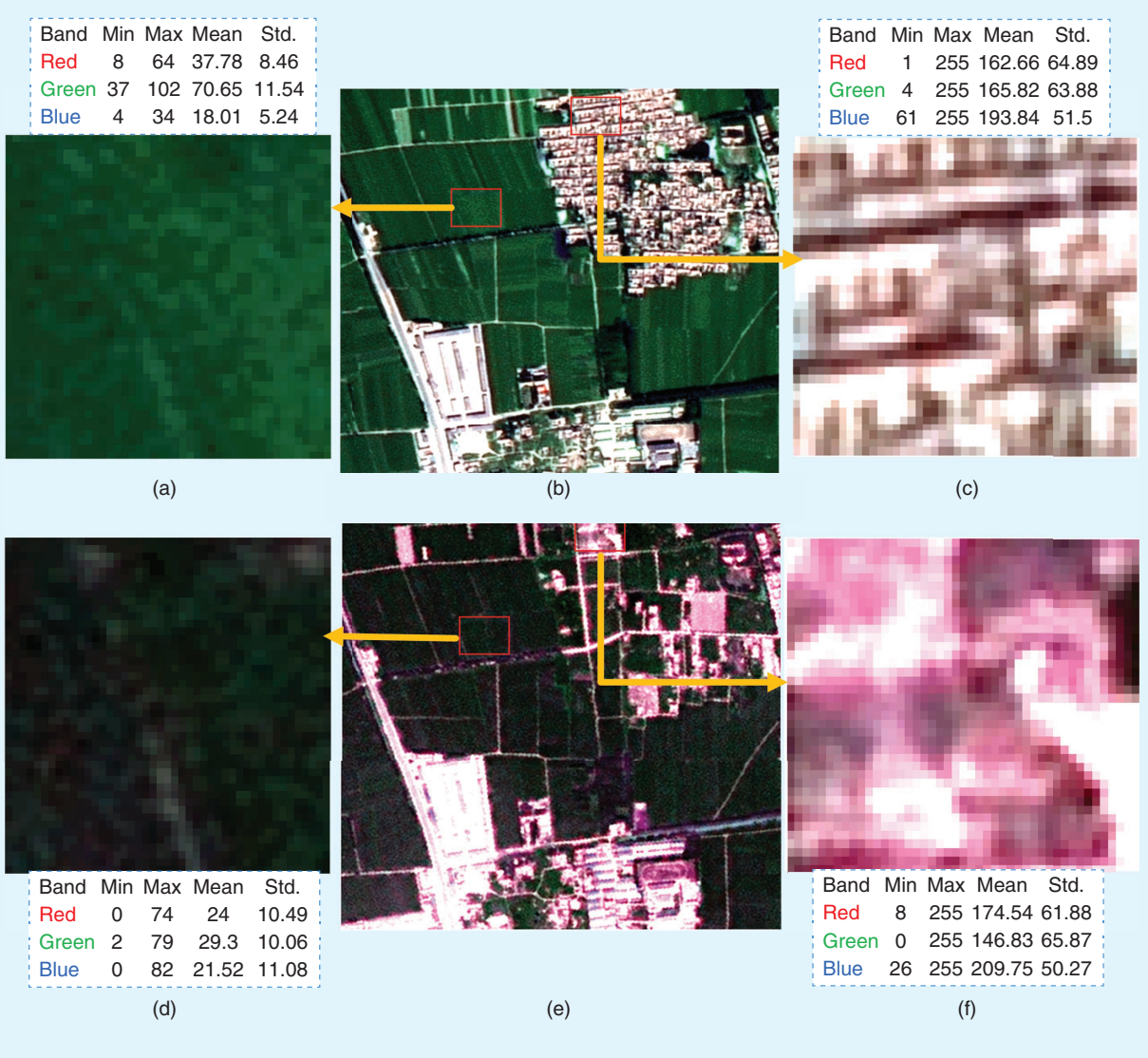


FIGURE 1. The characteristics of a sample VHR bitemporal image: the SPOT-5 satellite (a)–(c) pre-event and (d)–(f) postevent images with 2.5-m/pixel resolution. The (a) and (d) unchanged as well as (c) and (f) changed areas are shown. Max: maximum; Min: minimum; Std.: standard deviation.

threshold to divide the entire change magnitude image into changed and unchanged areas is a difficult task. These characteristics of VHR images limit the practical application of LCCD.

A VHR image generally has a fine resolution in the spatial domain and a coarse resolution in the spectral domain, but it can describe ground targets in detail in terms of their texture, structure, shape, and size. In recent decades, VHR remote sensing images have been used successfully in many practical applications, such as land cover classification [11], [12], scene classification [13]–[15], target change detection [16], [17], and LCCD [10], [18]. In this article, we concentrate on reviewing LCCD methods with VHR remote sensing images to provide an overview of the development in the methodology.

METHODOLOGY

Some rules must be defined to retrieve articles on LCCD using VHR remote sensing optical images from a database. In this study, several constraints were defined and applied to achieve the objective:

- All of the articles are indexed from the Web of Science (WoS) Core Collection database and were published from 2001 to 2019.
- The article titles should contain “very high resolution” or “VHR” and “change detection.” “Bitemporal images” or “remote sensing images” were used to refine the search results.
- If “object” and “change detection” were included in an article’s title, then the article would be selected for analysis because object-based techniques are generally employed for processing VHR images [19].

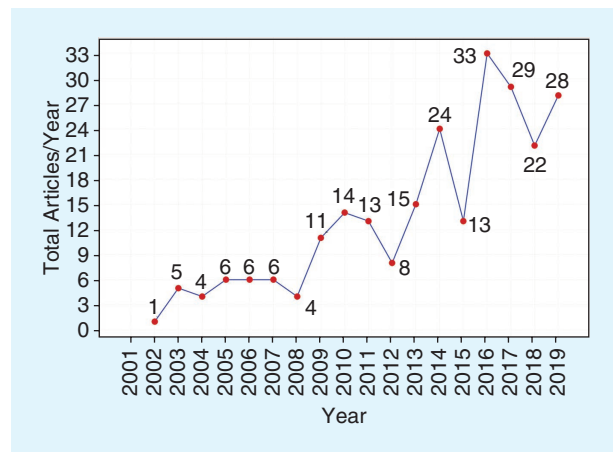


FIGURE 2. An overview of the articles referring to “change detection” and “VHR” images in WoS (through December 2019).

Unrelated topics referring to change detection based on synthetic aperture radar (SAR), biological, or x-ray images; land cover mapping; or target detection were manually excluded from the refined results because our report focuses on LCCD with VHR optical images. Some articles referring to LCCD without the keyword “change detection,” such as research on the updating of land cover maps [20] and building damages [21]–[23], are considered in our investigation.

Based on these criteria, 356 articles were selected after applying the constraints and excluding rules. Moreover, the total number of published articles on LCCD with VHR remote sensing images in each year increased from 2001 to 2019 (Figure 2). In these articles, LCCD with VHR optical images has been widely applied in many fields, such as building change detection, land cover mapping, and earthquake damage evaluation. In the present study, the workflow of LCCD with VHR bitemporal optical images is summarized in Figure 3. The general flowchart contains three major parts, namely, the preprocessing steps, exploration of neighboring context, and results of LCCD and performance assessment. Each part is discussed in the following sections.

REVIEW OF THE MAJOR TECHNIQUES OF LCCD WITH VHR OPTICAL IMAGES

IMAGE PREPROCESSING IN LCCD

LCCD usually refers to bitemporal or multitemporal images. Thus, preprocessing is required to reduce pseudochanges caused by geometry position errors and spectral reflectance phenological differences. Here, the two widely employed preprocessing steps for change detection are analyzed as follows.

In LCCD with VHR images, geometric coregistration between bitemporal images in terms of a geographical position is an important preprocessing task because misregistration will bring noise to the detection map [24], [25]. This problem has attracted considerable research attention. Marchesi et al. [26] proposed an LCCD technique with VHR

images sensitive to contextual information and robust to registration noise. Bovolo et al. [27] provided an adaptive estimation of registration noise distribution in multitemporal VHR images.

Han et al. [28] offered a method for the estimation of edge-based registration noise to improve the detection maps of LCCD with VHR images. Falco et al. [29] have developed a window-based method to minimize the misregistration error. Hence, coregistration, as a preprocessing task of LCCD with VHR images, has been studied by some researchers [30], [31].

However, coregistration between bitemporal images depends on the data preprocessing level. In general, ground control points (GCPs) are needed to achieve the coregistration, and GCPs are usually collected by data providers [32]. Collecting GCPs requires both field work and GPS equipment, and this is time consuming as well as labor intensive.

In addition to the preprocessing of coregistration, radiometric cocorrection between bitemporal images is required to reduce pseudochanges in LCCD [33]. For example, Bruzzone and Bovolo [34] stated that different types of radiation may cause pseudochanges in the detection results. Mura [35] emphasized that radiometric corrections should be applied to bitemporal images before conducting LCCD algorithms.

To solve this problem, scholars have developed many methods, such as radiometric normalization [36], linear radiometric normalization [37], histogram matching [38], and incorporating a metric learning approach [39]. Although many studies have mentioned radiometric cocorrection as a necessary preprocessing step of LCCD with VHR optical images, a quantitative analysis of radiometric cocorrection error in the change detection results is still unavailable. Furthermore, in practical applications, scholars assume that no significant radiometric difference exists between bitemporal images in LCCD [27], [30].

EXPLORATION OF NEIGHBORING CONTEXT

A number of studies have demonstrated that utilizing spatial contextual information can help improve the detection performance of LCCD with VHR optimal images [11], [40], [41]. This section summarizes the change detection methods and their main steps. The advantages and disadvantages are also discussed and analyzed. Table 1 presents a brief summary of the main LCCD techniques with VHR optical images. Many studies have indicated the lack of strict criteria for grouping LCCD methods [41]–[44]. In the present study, the approaches mentioned in the selected articles are classified into four branches according to their manner of exploration or utilization of spatial contextual information.

REGULAR NEIGHBORING CONTEXT

Table 1 defines *regular neighboring context* and presents two types of techniques for it, namely, regular geometry and the strict mathematical model. For example, local spectral trend

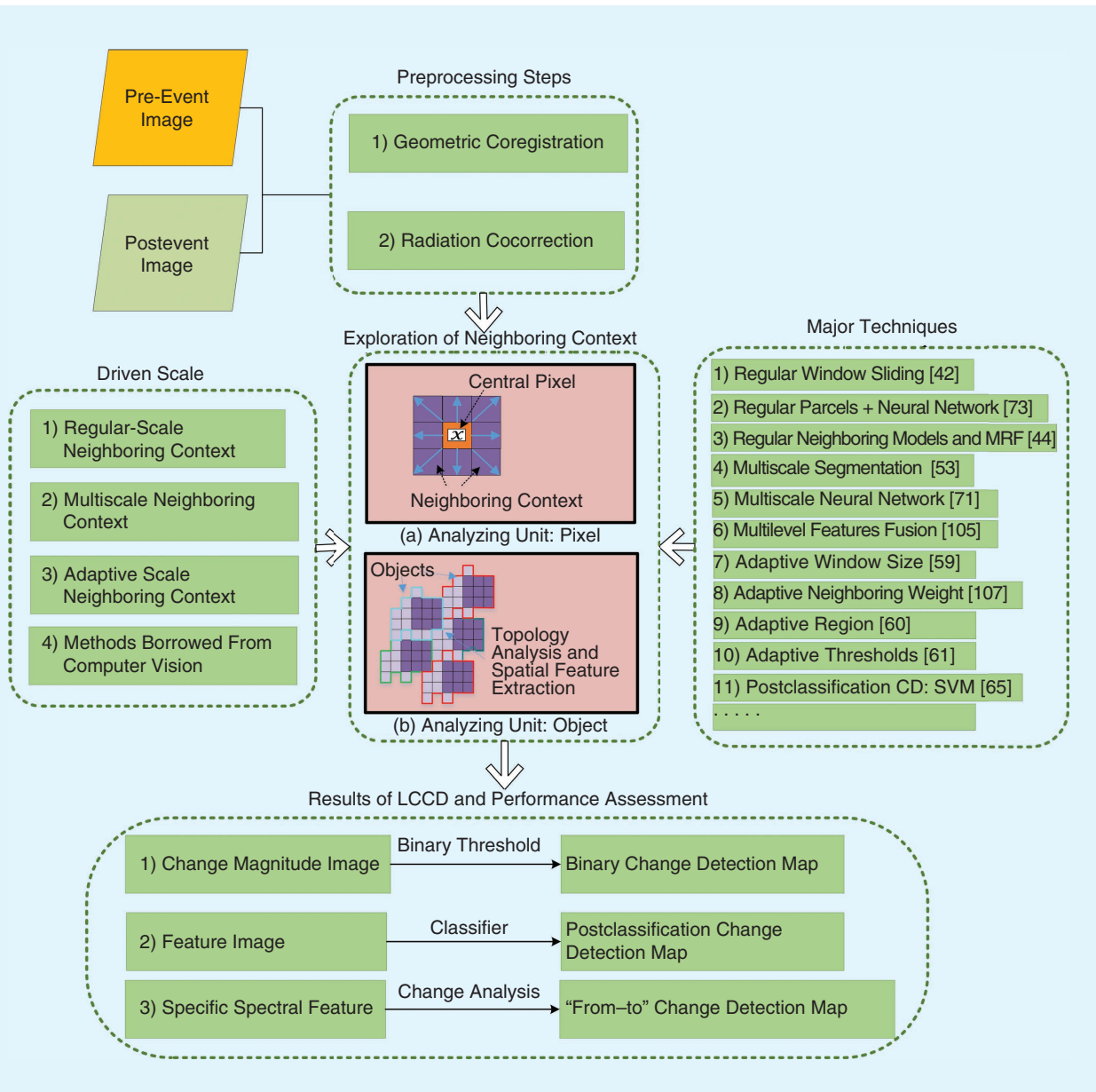


FIGURE 3. A general flowchart for LCCD with VHR optical images. CD: change detection; MRF: Markov random field; SVM: support vector machine.

similarity [69], [70], local texture [50], [71], gray-level cooccurrence matrices [71], [72]–[74], a windowed Fourier transform feature [75], and local probabilistic estimation [76] have been developed based on the sliding window method. In addition, regular structural elements coupled with morphological operations are widely used to extract neighboring contextual features in LCCD [18], [35], [77]–[79].

In recent years, many deep learning LCCD frameworks have been developed by dividing image pairs into regular blocks to utilize contextual information, based on such approaches as the convolutional neural network (CNN) [80]–[83], recurrent neural network (RNN) [84], deep belief network [85], generative adversarial network [86], Hopfield neural network [87], and UNet++ [88]. Moreover, deep

features were extracted with deep learning techniques in LCCD through deep change vector analysis [89] and normalized moment of inertia features [90].

In addition to constructing a regular geometry around a central pixel to explore neighboring contextual information, mathematical models are widely used to obtain invariant features around a central pixel and measure the change magnitude between pairwise images. Some examples of such mathematical models are Markov random field (MRF) [45], [48], [54], [91], conditional random field (CRF) [49], [92]–[95], and level set theory [96], [97]. From a critical perspective, the advantages and disadvantages of these methods based on regular neighboring context can be summarized as follows:

TABLE 1. A BRIEF SUMMARY OF THE MAIN LCCD TECHNIQUES WITH VHR OPTICAL IMAGES.

CHANGE DETECTION TECHNIQUES	DEFINITION AND MAIN TECHNIQUES	ADVANTAGES	DISADVANTAGES	MAIN REFERENCES
Regular neighboring context	This approach explores the contextual feature of a neighboring pixel by using regular geometry or strict mathematical models. The main techniques are sliding window, MRF, CRF, Gabor filter, and fuzzy clustering.	The method is easy to implement.	Various shapes and sizes of ground targets cannot be covered.	Bovolo and Bruzzone [45] Benedek et al. [46] Zheng et al. [47] Wei et al. [48] Zhou et al. [49] Li et al. [50]
Multiscale neighboring context	This method mines the spatial contextual feature in a multiscale manner. The main techniques are multiscale feature fusion, multiscale learning net, and object-based approaches.	The approach covers more shapes and sizes of ground targets, and more contextual information is explored.	Multiscale segmentation is usually required to generate multiscale objects. However, the parameter setting for segmentation techniques depends on experience.	Pacifci et al. [5] Janlipour and Taleai [51] Xu et al. [52] Zheng et al. [47] Chen et al. [53] Peng and Zhang [54] Lv et al. [55] Zhang et al. [56] Xiao et al. [57] Gil-Yepes et al. [58] Hussain et al. [59]
Adaptive neighboring context	This approach concentrates on the extraction of contextual information in an adaptive manner. The main techniques are adaptive window size, region, weight, and threshold.	The details of ground targets, such as the boundary, shape, and size, can be well preserved.	Parameter tuning is time consuming for a specific data set.	Kosugi et al. [60] Bovolo et al. [27], [61] Gong and Corpetti [62] Lv et al. [63] Solano-Correa et al. [64]
Methods borrowed from computer vision	This method focuses on exploring the geometry features of ground targets by mining the similarity of neighboring pixels. The main techniques are geometry feature extraction, 3D reconstruction, stereo matching, and local geometry descriptors.	The details of ground targets, such as the boundary, shape, and size, can be well preserved.	High quality of the data sets is necessary for supporting geometry feature exploration with computer vision techniques.	Radoi and Datcu [65] Champion et al. [66] Tang et al. [67] Xiao et al. [57] Liu et al. [17] Sui et al. [68]

- The use of regular neighboring context around a central pixel to cover the spatial contextual information is an intuitive and useful method.
- The regular shape of utilizing spatial contextual information has a tendency to blur the boundary between the topology-touched targets due to their varying shapes and sizes in a geographical area.
- Determining the optimal size of the neighboring geometry or group of optimal parameters for mathematical models or deep learning techniques while exploring contextual information for a given bitemporal image is time consuming.

MULTISCALE NEIGHBORING CONTEXT

Multiscale techniques can be used to obtain neighboring contextual information around a pixel in bitemporal VHR images (Table 1). In these techniques, contextual information around a pixel is exploited by multiscale objects [98], multiscale deep learning techniques [5], [99], and hierarchy scale methods [100]. The characteristics of these methods are summarized in this section.

First, object-based approaches have been widely used as multiscale techniques to effectively process VHR remote sensing images [101], [102]. In these techniques, the term *object* is defined as a group of pixels with homogeneous spectra and spatial continuity. Multiscale segmentation

should be conducted before applying object-based LCCD techniques to acquire "objects" from pixels.

In recent decades, many object-based methods have been developed for LCCD with VHR images. For example, object-level features were extracted to detect land cover change [10], [56], [103], [104]. Furthermore, object-based distance was developed to measure the change magnitude between pairwise and bitemporal images [55].

Object-based uncertainty analyses were also used in other studies [56], [105]. The relationship between an object and its topology was analyzed to detect land cover change [106]. Advancements in object-based LCCD methods depend on reducing noise and preserving boundaries [19], [107]. However, a prerequisite in the application of object-based LCCD methods is the use of multiscale segmentation algorithms to generate "objects."

Furthermore, the parameter setting of many multiscale segmentation algorithms is dependent on the user's experience [108]. Minor change targets are often missed in the application of object-based LCCD methods [59], [109], [110]. Maintaining consistency between the segmentation of bitemporal images is a challenge in object-based land cover detection [57].

Second, multiscale deep learning networks are popular when LCCD is applied on VHR images. These networks

include the multiscale CNN [53], [80], fuzzy neural network [111], Hopfield neural network [87], and multilayer RNN [84], [112]. Deep learning-based LCCD methods have the advantage of avoiding the generation of change magnitude images. Hence, the determination of binary thresholds for dividing the change magnitude images into binary change detection maps is optional because deep learning techniques can learn the “changed” and “unchanged” models directly from the training samples.

Despite the fact that realizing and extending the scale of training samples through rotating the direction of the samples can improve the robustness and performance of a network [18], the negative effect of the regular shape of image blocks is maintained in the detection maps. Furthermore, a network can obtain an expected detection map only with sufficient fully trained samples; however, labeling the change detection samples is time consuming and labor intensive [113].

Other multiscale techniques applicable to LCCD are the multiscale hierarchy LCCD framework [114], [115], multiscale morphological attribute profiles [78], multiscale morphological compressed change vector analysis (CVA) [77], and feature fusion driven by a multiscale segmentation voting decision [47], [116]. These hierarchy frameworks indicate the following possible ways of considering contextual information and improving the performance of LCCD with VHR images:

- ▶ Building a vector based on hierarchy scale features can improve the detection accuracy compared with using single-scale counterparts.
- ▶ Multiscale neighboring information can be exploited by assigning different values to the parameters of morphology operations.
- ▶ Exploring and fusing features from different scales or temporal images is beneficial to the improvement of detection performance with VHR remote sensing images.

ADAPTIVE NEIGHBORING CONTEXT

Adaptive neighboring context is another LCCD branch used to cover the various shapes and sizes of ground targets in a scene (Table 1). Compared with the previously mentioned branches, LCCD methods based on an adaptive neighboring context have the advantage of maintaining change details, such as boundary preservation [27], [63]. The shape of adaptive neighboring context can vary in consistency with the target boundary (Figure 4).

In adaptive region extension, the spectral difference between a central pixel and its neighbors should be less than T_1 , and the total number of assigned pixels around a seed pixel should be less than T_2 . The iterative extension is terminated until one of the constraint rules is not satisfied. Additional details about the relationship between an adaptive region and the parameters (T_1 and T_2) can be found in [63].

Many adaptive-scale-based LCCD methods have been developed in the past decades. These include methods based

on the adaptive window size [62], weight [56], region [63], [117], information fusion [6], MRF [48], threshold [64], and model [60] as well as the reduction of adaptive noise registration in LCCD [61]. In these methods, the relationship between a central pixel and its neighbor is measured with spectral similarity. The relationship is utilized to determine the adaptive window size, weight value, or region size.

Therefore, the influence of neighboring pixels on the central pixel varies with the spectral reflection of the ground target itself. One advantage of adaptive-scale LCCD methods lies in maintaining the shape of ground targets, improving the homogeneity, and preserving the details of the change area. However, the parameter tuning of adaptive-scale methods is generally required in practical application.

OTHER METHODS FROM COMPUTER VISION

In addition to the mentioned LCCD methods, computer vision techniques, such as the binary descriptors algorithms [65] and building boundary descriptors [17], [57], [66], [67], are attractive in terms of achieving LCCD with VHR optimal images. From the viewpoint of computer vision, numerous studies have concentrated on the coregistration of bitemporal images to guarantee the quality and performance of change detection [118]. Moreover, scene change

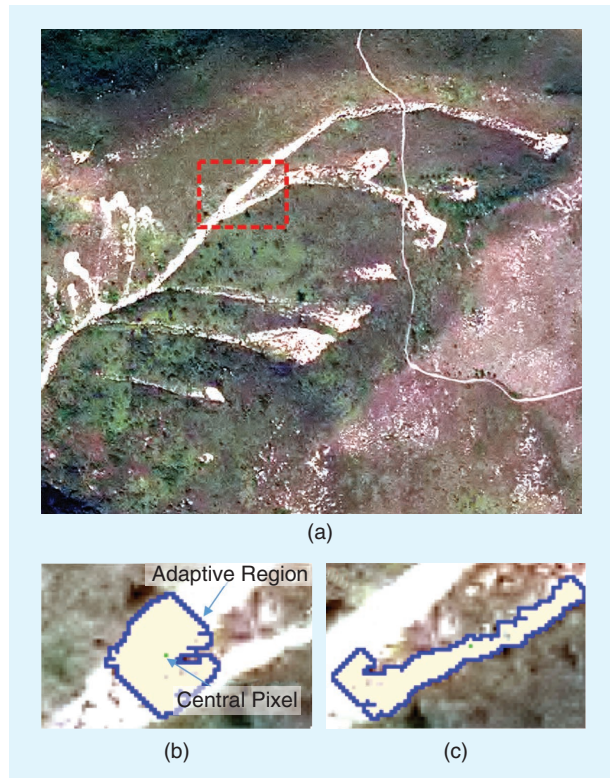


FIGURE 4. A demonstration of the adaptive ability of regions in describing the boundary of (a) the landslide area (in the red box) using thresholds T_1 and T_2 ; (b) $T_1 = 10$ and $T_2 = 500$ as well as (c) $T_1 = 10$ and $T_2 = 1,000$. The green pixel denotes the seed pixel of each adaptive region. The blue contour indicates the adaptive region. (Source: [63].)

detection has been popular in the application of VHR optical images [119]–[121].

Many widely used computer vision techniques, such as line feature extraction [68], 3D reconstruction [122]–[124], and stereo matching [125]–[127], have been adopted to achieve LCCD with VHR optical images. The literature review revealed that computer vision techniques usually focus on LCCD with a single kind of ground object, such as buildings or roads, especially for 3D objects. One advantage of computer vision-based LCCD approaches lies in detecting the details of ground objects using local descriptors and geometric features [128]. However, other data sets, based on SAR [129], lidar [130], and digital surface models [123], are usually required to be coupled with optimal images to achieve LCCD tasks.

RESULTS OF THE LCCD AND PERFORMANCE ASSESSMENT

Two kinds of change detection maps exist in practical applications. The first major type is called the *binary change detection map*, and it can only describe the shape, size, and distribution of land cover change. The other is called the *multitask change detection map* [100], [131], [132] it can provide “from-to” change information. In this approach, change detection is achieved by directly comparing the classification maps of different temporal images.

In addition to multitask change detection methods, “from-to” change information can be acquired through the feature analysis of ground targets. For example, Wen et al. [133] proposed multiple indices and measured the transformation among different classes in terms of multi-index features. Aleksandrowicz et al. [134] used the normalized difference vegetation index and texture to build a class transformation and change matrix. Volpi et al. [71] adopted a nonlinear classifier (support vector machine) to cope with high intraclass variability.

Binary change detection is the most widely used in the family of LCCD with VHR optical images. In addition, one advantage of postclassification-based LCCD methods is their ability to provide “from-to” change information. However, the detection accuracy and performance depends on the classification performance, and the large intraclass variations in VHR images led to difficulty in distinguishing among different classes [9]. Although the analysis of feature difference among different ground targets in bitemporal images can determine the “from-to” change transformation, these methods require bitemporal images to have almost the same acquisition season and imaging condition and, thus, reduce the pseudochange from the phenology impact.

In summary, accuracy assessment is a quantitative measurement to compare and test the performance of an algorithm. Intuitively, this quantitative measurement is achieved by comparing the result of an algorithm with the corresponding ground truth map (GTM). After the indicators employed in the literature were reviewed [135]–[138],

nine widely used indicators were selected and are summarized in Table 2, where the formula and definition of each indicator are detailed. Some symbols need to be defined here to explain the evaluation indicators. TP and TN denote pixels correctly detected as “changed” and “unchanged,” respectively. FP and FN indicate the respective false changed and unchanged pixels in the detection map of an approach.

By analyzing the definition of each formula, it can be observed that different indicators have an unequal bias for evaluation, and the performance of a specific algorithm may be better or worse than the one of other methods, depending on the indicator. In numerous practical applications and performance assessments of algorithms, three of the nine indicators are usually selected to assess the performance of an algorithm (i.e., FA , MA , and Ka were adopted in [34] and [50]; CR , CP , and QA were used for the quantitative comparison of landslide inventory mapping in [139] and [140]; and OA , AA , and Ka were used in [141]).

EXPERIMENTS

To investigate the performance of LCCD approaches in comparison with VHR optical images, this section compares eight widely used approaches, including three unsupervised methods (CVA_MRF [142], multiresolution level set (MLS) [140], and deep change vector analysis (DCVA) [89]) and five supervised methods [principal component analysis- k -means (PCA_Kmeans) [143], CVA_fuzzy c-means (FCM) [144], level set evolution with local uncertainty constraints (LSELUC) [145], sorted histogram (SH) [146], and key point vector distance (KPWD) [147]]. The algorithms were applied to three multitemporal data sets, all depicting real landcover changes. Data set A was collected by the QuickBird satellite over an area of urban development in the city of Ji Nan in the Shan Dong province of China. Data sets B and C are airborne acquisitions showing changes in the landscape due to landslide events occurred in Lantau Island in Hong Kong. The scenes and details of each data set, including the spatial resolutions, are reported in Figure 5.

The performance of each algorithm was evaluated by using the nine indicators described in Table 2, the results of each approach are reported in Tables 3–5, and the obtained change detection maps are shown in Figures 6–8. The results of these investigations reveal the following insights:

- In general, different methods vary in terms of their performance on a particular data set. However, the investigations also indicate that one specific approach may obtain different accuracies when applied on different data sets because the separability between the changed area and background for different data sets varies with different image scenes.
- Different indicators have different bias evaluations. For example, for data set A, the LSELUC approach [145] achieved the highest accuracy in terms of OA , CVA_MRF [142] presented the greatest accuracy in terms of CP , and DCVA [89] obtained the best accuracy in terms

TABLE 2. A DESCRIPTION OF EVALUATION INDICATORS FOR QUANTITATIVE COMPARISON.

EVALUATION INDICATORS	FORMULA	EXPLANATION
False alarm (FA)	$FA = \frac{FP}{TN + FP}$	The ratio between the number of pixels that are detected as "changed pixels" but are unchanged in the GTM and the number of the pixels that are unchanged in the GTM.
Missing alarm (MA)	$MA = \frac{FN}{TP + FN}$	The ratio between the number of pixels that are identified as "unchanged" but are changed in the GTM and the number of pixels that are changed in the GTM.
Total error (TE)	$TE = \frac{TP + TN}{TP + TN + FP + FN}$	The ratio between the number of pixels that are identified as "unchanged" but are changed in the GTM and the number of pixels that are changed in the GTM.
Overall accuracy (OA)	$OA = \frac{TP + TN}{TP + TN + FP + FN}$	The ratio between the number of correctly detected pixels in the result and the total number of the GTM.
Kappa coefficient (Ka)	$P_e = \frac{(TP + FP) \times (TP + FN) + (FN + TN) \times (FP + TN)}{(TP + TN + FP + FN)^2}$ $Ka = \frac{OA - P_e}{1 - P_e}$	P_e represents the results of the previous equation. Ka reflects the reliability of the detection map by measuring the interrater reliability for the changed and unchanged items for LCCD.
Average accuracy (AA)	$AA = \frac{1}{2} \times \left(\frac{TP}{TP + FP} + \frac{TN}{TN + FN} \right)$	The AA is for two ratios: one is the ratio between the true changed pixel in the results and the changed pixel in the GTM, and the other is the ratio between the true unchanged pixel in the results and the unchanged pixels in the GTM.
Completeness (CP)	$CP = \frac{TP}{TP + FN}$	The ratio between the number of changed pixels that are correctly identified and the number of the pixels that are changed in the GTM.
Correctness (CR)	$CR = \frac{TP}{TP + FP}$	The ratio between the number of changed pixels that are correctly identified and the total number of changed pixels in the result.
Quality (QA)	$QA = \frac{TP}{TP + FP + FN}$	The ratio between the number of changed pixels that are correctly identified and the number of total changed pixels in the results and GTM.

FN: false negative; FP: false positive; TN: true negative; TP: true positive.

of FA. Therefore, many different evaluation indicators are expected to be included for a more comprehensive performance assessment of LCCD with optical images. From the visual observations (Figures 6–8), it can be observed that 1) different approaches have varying performances on the disparate data sets and 2) different methods have various accuracies for a specific data set in terms of varying indicators. This visual performance conclusion well supported the quantitative comparisons in Tables 3–5.

DISCUSSION

To obtain an overview of the development of LCCD with VHR optical images, we statistically analyzed the articles referred to. In accordance with the perspective and focus of these articles, we discussed LCCD with VHR optical images from the following viewpoints: technology, application, data sets, and accuracy assessment. The details of this quantitative analysis are presented in the following sections.

TECHNIQUES

As mentioned in the previous section, here, we dichotomized the major LCCD methods into four groups in terms of different manners of utilizing spatial contextual information: regular neighboring context [45]–[48], multiscale neighboring context [5], [51]–[53], adaptive neighboring context [27], [60], [61], and other methods borrowed from

computer vision. As shown in Figure 9, the regular and multiscale context-based approaches account for 31.7% and 45.2% of the total articles, respectively. However, the adaptive context-based approaches account for only 14.6% of the total quantity. The discrepancy could be due to the fact that more than two parameters are required by an algorithm that explores adaptive context [27], [63], [148].

Moreover, the optimal parameter's setting of an adaptive context exploration algorithm for a specific data set remains a challenge [6], [27], [60]. In practical applications, trial-and-error approaches are usually adopted for identifying the optimal set of parameters for a given data set and a specific algorithm. Hence, multiscale context-based LCCD approaches play a dominant role in the technical development of LCCD with VHR images. Moreover, adaptive context requires more attention in terms of obtaining the optimized parameters and improves the degree of the model automatically for the practical application of LCCD with VHR optimal images.

APPLICATIONS

LCCD with VHR images has been widely used in practice [33], [41], [149]. In this section, we refined the 356 articles from the viewpoint of application for thematic analysis. Figure 10 illustrates that many LCCD applications with VHR optical images focus on urban LCCD.

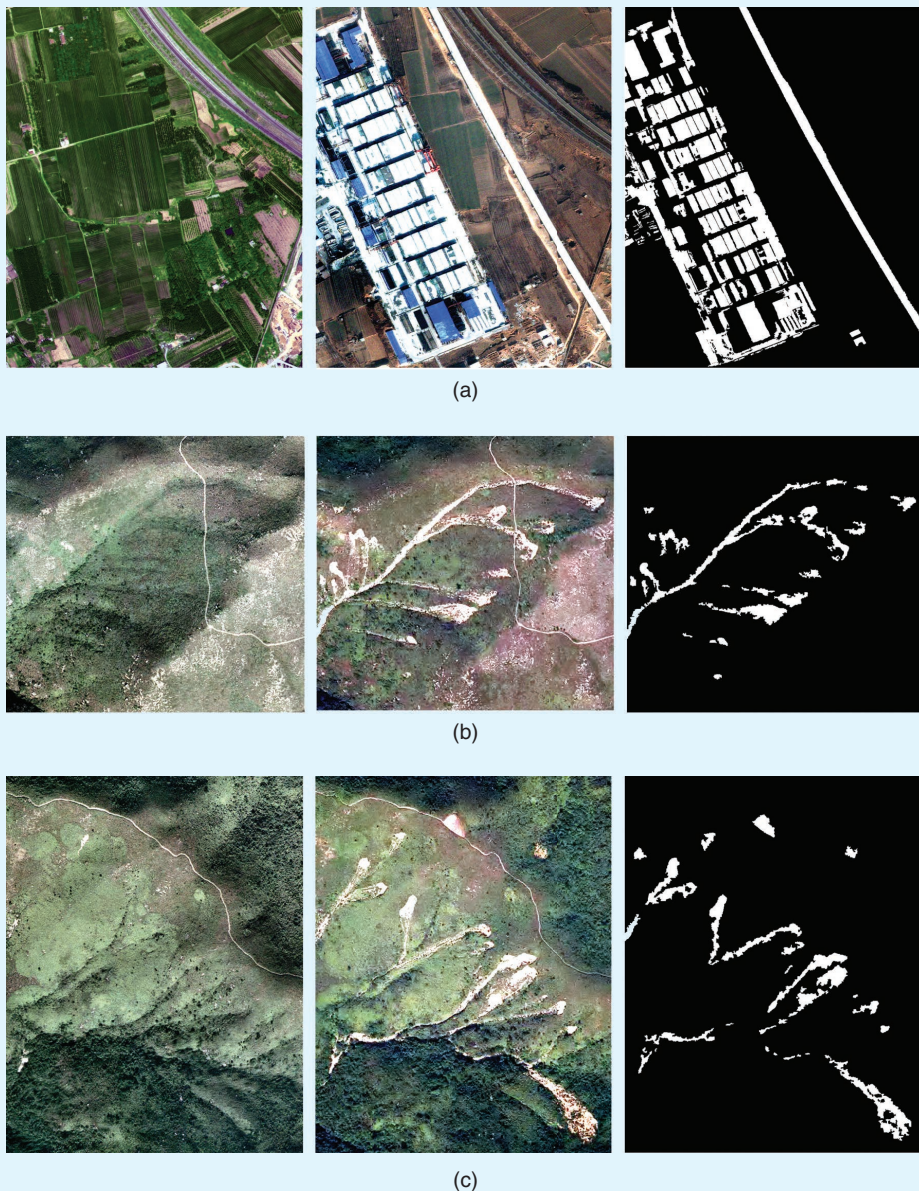


FIGURE 5. Three pairs of bitemporal VHR images for quantitative comparisons of different LCCD methods: (a) date 1: April 2007; date 2: February 2009; location: JiNan, China; resolution: 0.61 m/pixel; and ground reference: 601449/2961051; (b) date 1: April 2007; date 2: July 2014; location: Hong Kong, China; resolution: 0.5m/pixel; and ground reference: 25672/496704; and (c) date 1: April 2007; date 2: July 2014; location: Hong Kong, China; resolution: 0.5 m/pixel; and ground reference: 35066/677434.

Based on these observations, 92 study areas were located in the urban region, accounting for 30% of the total quantity. In addition, building change detection played an important role in change detection with VHR optical images, accounting for 23.8% of the 307 applications in the 356 articles. However, the application of such methods to disaster change detection, such as earthquake and landslide inventory mapping, has not gained sufficient attention, probably because of the difficulty of acquiring pre- and postevent images for natural disaster events. Furthermore, coregistration between bitemporal images

becomes challenging because land cover disasters, such as landslides and earthquakes, usually result in the deformation of ground elevation.

DATA SETS

Data sets are important in investigating the performance of LCCD algorithms. If an algorithm adapts to more kinds of data sets with different resolutions, then it may have better adaptability and robustness [73]. Thus, we reviewed the data sets mentioned in the selected articles in terms of data sourcing and size of the study areas. Figure

TABLE 3. A COMPARISON AMONG SELECTED METHODS FOR DATA SET A.

METHOD	FA	MA	TE	OA	Ka	AA	CP	CR	QA
CVA_MRF [142]	22.92	2.11	18.81	81.19	0.8041	87.48	97.89	51.26	50.69
MLS [140]	8.71	13.26	9.61	90.39	0.9004	89.01	86.74	71.03	64.07
DCVA [89]	7.38	33.58	11.8	88.2	0.8748	79.52	66.42	64.64	48.72
PCA_Kmeans [143]	11.47	17.32	12.63	87.37	0.8677	85.6	82.68	63.96	56.4
CVA_FCM [144]	22.75	2.14	18.68	81.32	0.8055	87.56	97.86	51.44	50.87
LSELUC [145]	9.41	10.4	9.6	90.4	0.9008	90.09	89.6	70.11	64.83
SH [146]	8.77	33.78	13.71	86.29	0.8529	78.72	66.22	65.02	48.82
KPVD [147]	10.10	14.68	11	89	0.8855	87.61	85.32	67.54	60.51

Ka is within the range of zero to one, and the other indicators are presented as percentages.

TABLE 4. A COMPARISON AMONG SELECTED METHODS FOR DATA SET B.

METHOD	FA	MA	TE	OA	Ka	AA	CP	CR	QA
CVA_MRF [142]	17.38	11.2	17.06	82.94	0.827	85.71	88.8	21.47	20.9
MLS [140]	7.6	14.55	7.95	92.05	0.9196	88.93	85.45	37.57	35.31
DCVA [89]	8.76	19.14	9.29	90.71	0.9059	86.05	80.86	33.06	30.66
PCA_Kmeans [143]	3.8	11.82	4.2	95.8	0.9576	92.19	88.18	55.41	51.57
CVA_FCM [144]	17.38	11.20	17.06	82.94	0.827	85.71	88.80	21.47	20.9
LSELUC [145]	3.16	9.69	3.49	96.51	0.9649	93.57	90.31	60.46	56.77
SH [146]	17.34	25.31	17.74	82.26	0.8188	78.67	74.69	18.73	17.61
KPVD [147]	1.34	15.43	2.06	97.94	0.9792	91.61	84.57	77.09	67.58

Ka is within the range of zero to one, and the other indicators are presented as percentages.

TABLE 5. A COMPARISON AMONG SELECTED METHODS FOR DATA SET C.

METHOD	FA	MA	TE	OA	Ka	AA	CP	CR	QA
CVA_MRF [142]	19.28	16.11	19.13	90.87	0.8055	82.30	83.89	18.38	17.75
MLS [140]	7.48	20.8	8.13	91.87	0.9176	85.86	79.2	35.42	32.4
DCVA [89]	18.14	31.1	18.78	81.22	0.8078	75.38	68.9	16.43	15.3
PCA_Kmeans [143]	2.51	19.43	3.35	96.65	0.9662	89.03	80.57	62.39	54.23
CVA_FCM [144]	19.6	15.94	19.42	80.58	0.8025	82.23	84.06	18.17	17.56
LSELUC [145]	2.34	15.67	2.99	97.01	0.9698	90.99	84.33	65.12	58.09
SH [146]	0.7453	55.18	3.43	96.58	0.9648	72.04	44.82	75.68	39.17
KPVD [147]	0.5344	15.37	1.27	98.74	0.9873	92.05	84.63	89.13	76.71

Ka is within the range of zero to one, and the other indicators are presented as percentages.

11 demonstrates that approximately nine kinds of data, including QuickBird, aerial orthophotos, WorldView, IKONOS, GaoFen, SPOT, GeoEye, UAV images, and others (ZY-3, Beijing-2, and Pleiades), were mentioned in the selected articles. QuickBird was the most widely used data set, accounting for 35.0% of the total quality. However, many images, including UAV and GeoEye images, were neglected.

In addition, the size of the study areas mentioned in the articles is reviewed. Area units were measured in square kilometers, and five ranges were divided for quantitative analysis,

namely, $0 < S \leq 5$, $5 < S \leq 10$, $10 < S \leq 15$, $15 < S \leq 20$, and $S > 20 \text{ km}^2$, where S denotes the study area size (Figure 12). The statistics showed that the areas mentioned in the investigations of the algorithms (about 76.6% in total quality) measured fewer than 5 km^2 . The majority of the current studies concentrated on promoting novel algorithms and have not yet verified the algorithms with large scene images.

That is because, in general, for specific geographical areas, the complexity of spatial certainty increases with an increase in the size of a geographic area [150], [151]. Thus,

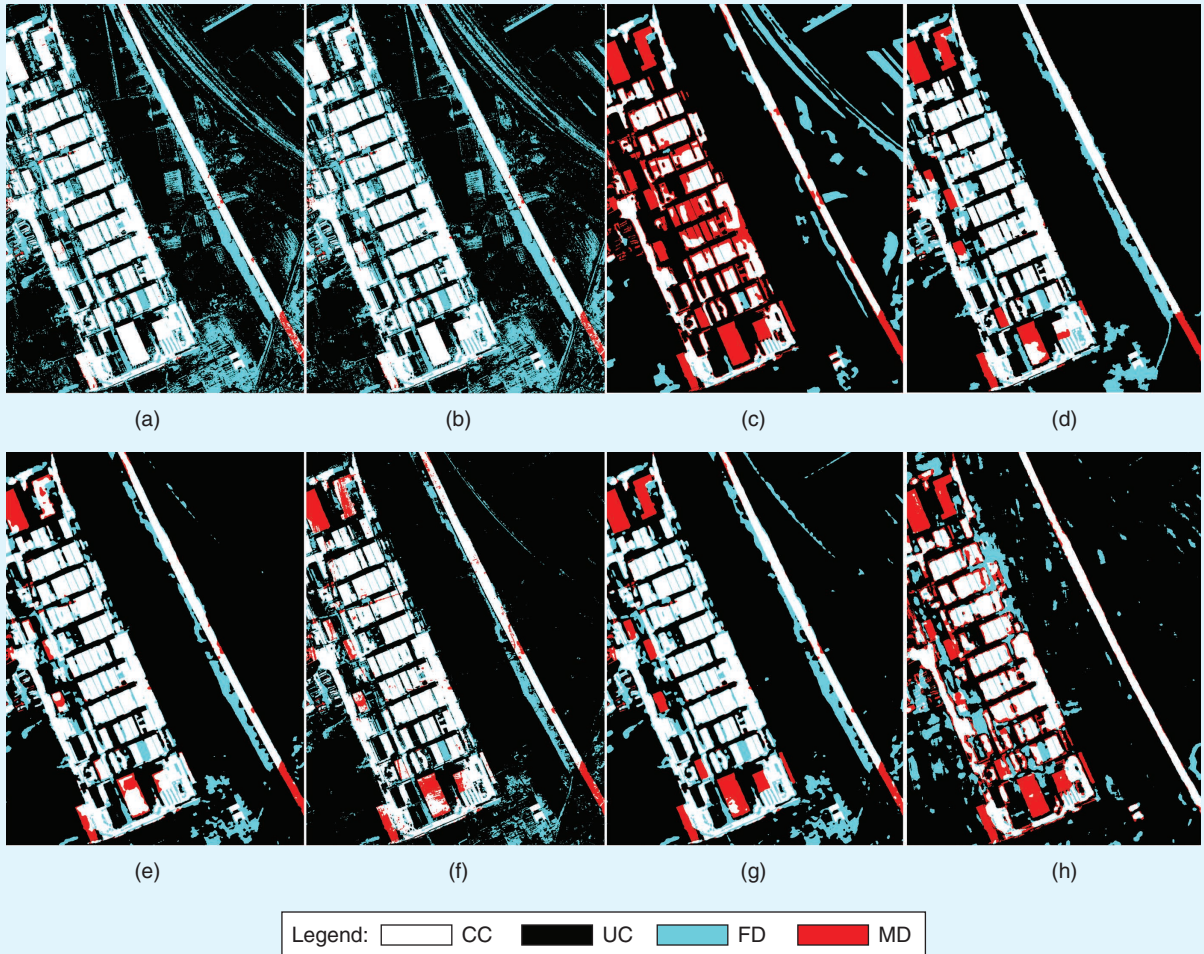


FIGURE 6. The binary change detection maps with different methods for data set A: (a) CVA_FCM [144], (b) CVA_MRF [142], (c) DCVA [89], (d) KPVD [147], (e) LSELUC [145], (f) MLS [140], (g) PCA_Kmeans [143], and (h) SH [146]. CC: corrected changed; FD: false detection; MD: missed detection; UC: unchanged.

from the perspective of practical applications of LCCD on VHR remote sensing images, the usability of the majority of LCCD algorithms still requires further investigation with large areas of data sets.

ACCURACY ASSESSMENT

The quantitative accuracies of each approach and data set in the experimental section well demonstrated that it is difficult to mark one method as “good” or “bad” in terms of the nine assessment indicators. For example, for data set A, the developed DCVA [89] achieved the best accuracy in terms of FA, yet CVA_MRF [142] obtained the best accuracy in terms of MA. However, evaluating the performance of an algorithm of LCCD with VHR optimal images should use additional indicators for a more comprehensive and objective assessment because doing so provides a potential guide to meet the preferred application of an algorithm’s user.

CHALLENGES AND OPPORTUNITIES OF LCCD WITH VHR IMAGES

Despite the numerous approaches for LCCD with VHR images that have been developed, challenges still exist in practical applications. In this study, these were mentioned from the viewpoint of practitioners, and opportunities were discussed from the perspective of researchers. The details of the challenges and opportunities are presented as follows:

- **Radiometric cocorrection requires additional attention:** Despite the availability of various LCCD techniques, radiometric cocorrection is required for images used in LCCD. The effect of radiometric cocorrection between bitemporal images on the accuracy of change detection maps still requires further investigation. Bitemporal images used in LCCD are usually acquired on different dates, and the process may vary in terms of sun height, atmospheric conditions, and even the phenology season. Thus, a radiometric difference exists between bitempo-

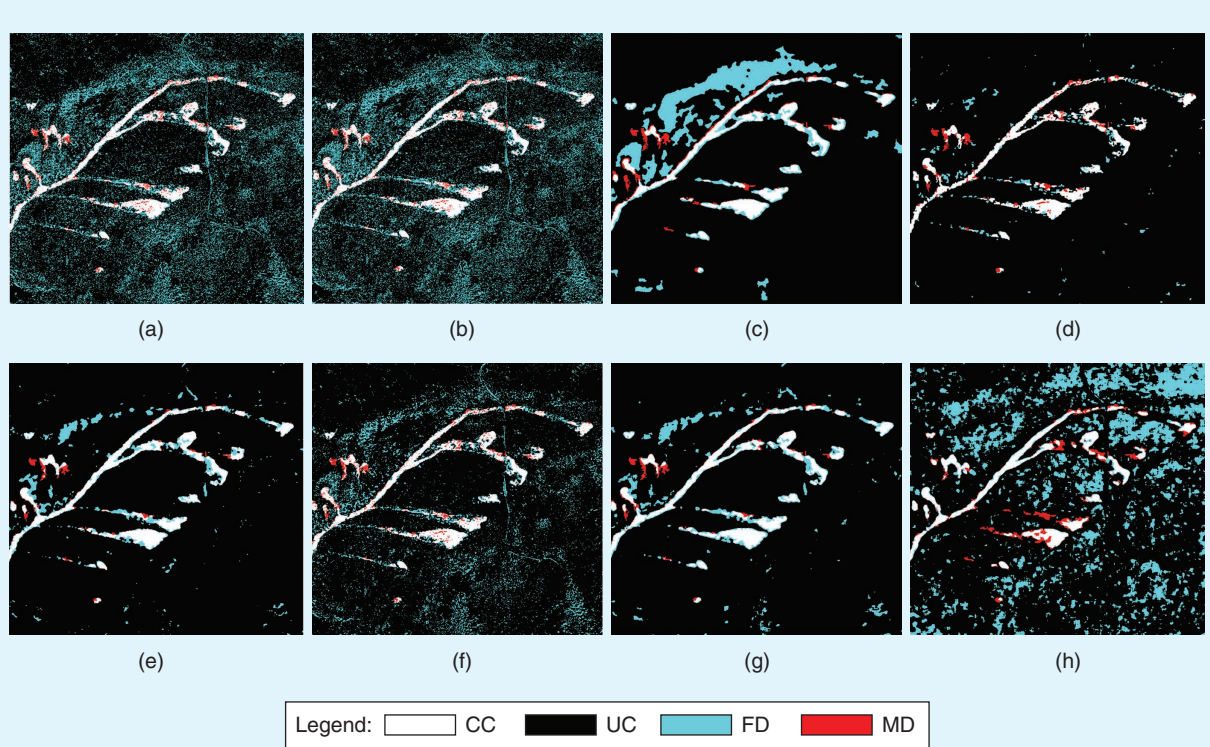


FIGURE 7. The binary change detection maps with different methods for data set B: (a) CVA_FCM [144], (b) CVA_MRF [142], (c) DCVA [89], (d) KPVD [147], (e) LSELUC [145], (f) MLS [140], (g) PCA_Kmeans [143], and (h) SH [146].

ral images. The radiometric cocorrection of noise should be considered in comprehensive analyses to promote the development of the method and reduce the radiometric difference between bitemporal images in LCCD.

- *LCCD based on bitemporal images with different resolutions is attractive in practical applications:* In the selected 356 articles, only two mentioned different resolutions in LCCD with VHR images [146], [152]. However, the resolution of images has been improved and refined due to the rapid development of sensor and satellite technology. Numerous practitioners have encountered many bitemporal images acquired by different platforms with varying resolutions. Therefore, investigating LCCD with different resolutions of VHR images and developing the corresponding solutions is important for practical applications.
- *The automation of LCCD methods must be improved for practical applications:* Regardless of the approaches, i.e., regular context, multiscale contexture, or adaptive-scale context-based approaches, the selection of optimal parameters requires trial-and-error experiments. However, this progress is time consuming and depends on the experience of practitioners. Therefore, simplifying the parameter setting or estimating parameters for automation is another challenge in LCCD with VHR images.
- *Change trend analysis and prediction with VHR images will become an interesting topic in future studies:* In addition to

developments in LCCD with low- and medium-resolution images and the accumulation of long-term series of VHR images for an area, monitoring the change trend for some interesting targets, such as the growth of urban buildings and urban green spaces, in a geographical area is necessary. Observing such changes with long-term series of VHR images and acquiring their change trend and pattern is beneficial for decision making.

CONCLUSION

LCCD with VHR optical images plays an important role in remote sensing. This approach provides an opportunity to discover, describe, and analyze land cover changes on Earth's surface. The rapid development of remote sensing platforms has provided the convenient availability of VHR remote sensing images. VHR optical images have become an important data source for the detection of land cover change. Designing advanced algorithms for these images is necessary to increase the popularity of change detection with VHR images and their potential applications in practical engineering.

In this article, the problems of LCCD with VHR remote sensing images were reviewed and analyzed in terms of algorithms, data sets, and applications. Challenges and opportunities were then discussed. Our study provides an overview of the available LCCD methods with VHR remote sensing images. Furthermore, the characteristics of the

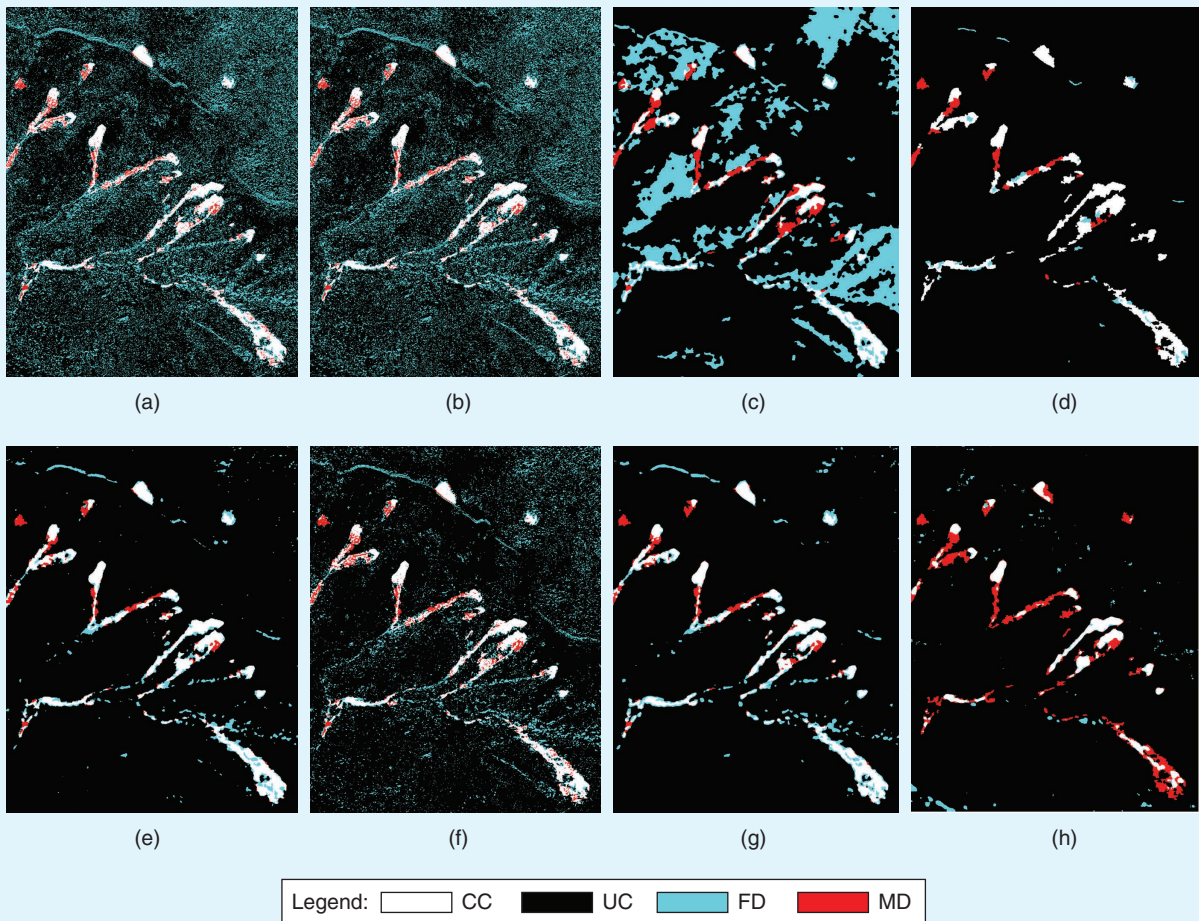


FIGURE 8. The binary change detection maps with different methods for data set C: (a) CVA_FCM [144], (b) CVA_MRF [142], (c) DCVA [89], (d) KPVD [147], (e) LSELUC [145], (f) MLS [140], (g) PCA_Kmeans [143], and (h) SH [146].

study areas mentioned in the corresponding methods in the literature, such as data sources and size, were quantitatively analyzed. Results may provide an objective assessment for future investigations.

In general, many issues, such as implementing an advanced radiometric cocorrection method in the preprocessing of bitemporal images to reduce a radiometric difference, still require further investigation and analysis. Almost all object-based LCCD methods focus on utilizing low-level object-based features of a single object, such as the spectral mean, textural characteristics, and other statistical features. High-level features, such as the topology of an object and its neighbors, should be extensively analyzed in future studies. Furthermore, time series images of an area have become available, and time series change detection and change trend analysis must be considered in LCCD with VHR remote sensing images.

ACKNOWLEDGMENTS

The authors would like to express their gratitude to the editor-in-chief, associate editor, and reviewers for their

insightful comments and suggestions. This work was supported by the National Natural Science Foundation of China (61701396 and 61801380) and the Natural Science Foundation of Shaan Xi Province (2018JQ4009). The corresponding author is Zhiyong Lv.

AUTHOR INFORMATION

Zhiyong Lv (lvzhiyong_fly@hotmail.com) received his M.S. and Ph.D. degrees from the School of Remote Sensing and Information Engineering from Wuhan University, China, in 2008 and 2014, respectively. He was an engineer of surveying and worked in The First Institute of Photogrammetry and Remote Sensing from 2008 to 2011. He is currently working with the School of Computer Science and Engineering, Xi'an University of Technology, Xi'an, 710048, China. His research interests include multihyperspectral and high-resolution remotely sensed image processing, spatial feature extraction, neural networks, pattern recognition, and deep learning and remote sensing applications. He is a Member of IEEE.

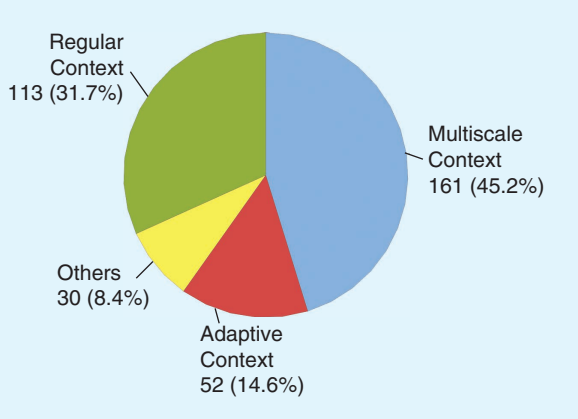


FIGURE 9. The statistics for LCCD as the subject of articles on VHR optimal images published in 2001–2019 from the viewpoint of techniques.

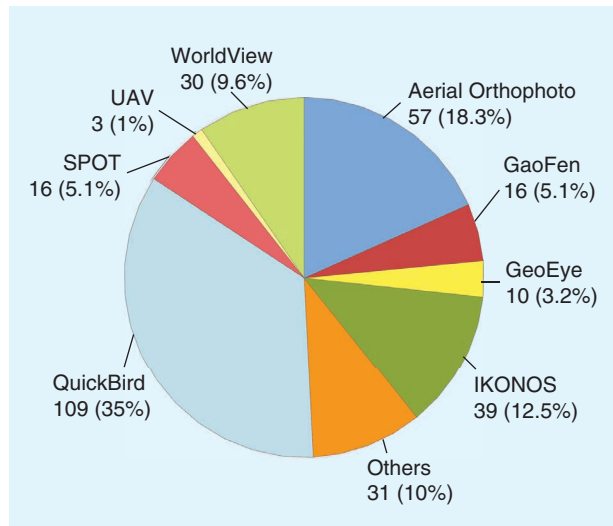


FIGURE 11. The statistics for LCCD as the subject of articles on VHR optimal images published in 2001–2019 from the viewpoint of data set sources. Among the 356 selected articles, 311 experiments mentioned data sources.

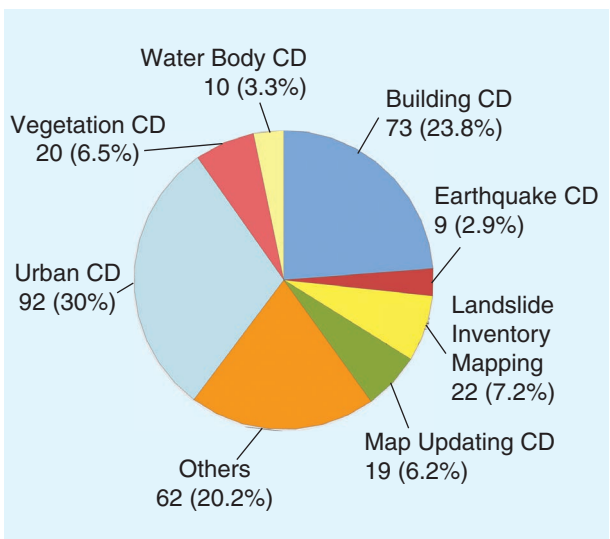


FIGURE 10. The statistics for LCCD as the subject of articles on VHR optimal images published in 2001–2019 from the viewpoint of applications. In the 356 articles, 307 experiments mentioned the characteristic of studying the area.

Tongfei Liu (liutongfei_home@hotmail.com) received his master's degree from Xi'an University of Technology, Shaanxi, China, in 2020. He is currently pursuing a Ph.D. degree in the School of Electronic Engineering, Xidian University, Xi'an, 710071, China. His research interests include in deep learning, computational intelligence, spatial-spectral feature extraction, pattern recognition, ground target detection, and land cover/land use change detection and classification through VHR remote sensing images (including satellite and aerial images). He is a Student Member of IEEE.

Jón Atli Benediktsson (benedikt@hi.is) received his Cand.Sci. degree in electrical engineering from the University of Iceland, Reykjavik, in 1984, and his M.S.E.E. and Ph.D. degrees in electrical engineering from Purdue University, West Lafayette, Indiana, in 1987 and 1990, respectively.

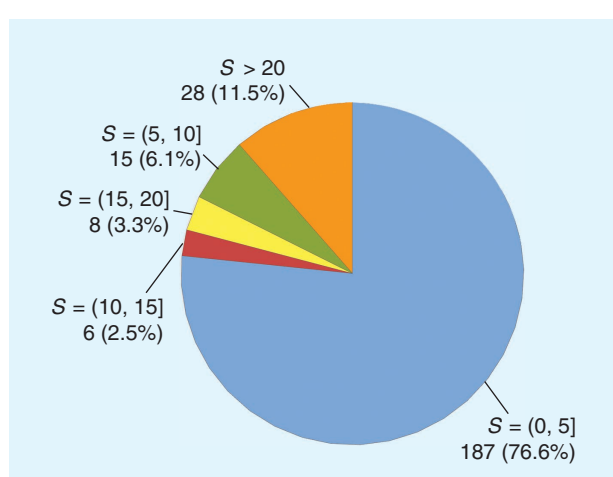


FIGURE 12. The statistics for LCCD as the subject of articles on VHR optimal images published in 2001–2019 from the viewpoint of study area sizes. In the 356 selected articles, 244 records mentioned the area sizes in experiments.

Since 2015, he has been the president and rector of the University of Iceland, Reykjavik, IS 107, Iceland, and he is a co-founder of the biomedical start-up company Oxymap. He was the 2011–2012 president of the IEEE Geoscience and Remote Sensing Society (GRSS) and has been on the GRSS Administrative Committee since 2000. He was the editor-in-chief of *IEEE Transactions on Geoscience and Remote Sensing* (TGRS) from 2003 to 2008 and has served as an associate editor of TGRS since 1999, *IEEE Geoscience and Remote Sensing Letters* since 2003, and *IEEE Access* since 2013. His research interests include remote sensing, the biomedical analysis of signals, pattern recognition, image processing, and signal processing. He is a Fellow of IEEE and a fellow of the Society of Photo-Optical Instrumentation Engineers.

Nicola Falco (nicolafalco@lbl.gov) received his B.Sc. and M.Sc. degrees in telecommunication engineering from the University of Trento, Italy, in 2008 and 2011, respectively. He holds a joint Ph.D. degree in electrical and computer engineering from the University of Iceland and information and communication technologies from the University of Trento, obtained in 2015. He is currently a senior scientific engineering associate at Lawrence Berkeley National Laboratory in the Climate and Ecosystem Sciences Division, Berkeley, California, 94720, USA. He received the recognition of *IEEE Geoscience Remote Sensing Letters* Best Reviewer in 2013 and was a corecipient of third place in the Student Paper Competition of the 2015 IEEE International Geoscience and Remote Sensing Symposium. He is a referee for several international journals, including *IEEE Transactions on Geoscience and Remote Sensing*, *IEEE Geoscience and Remote Sensing Letters*, and *IEEE Journal of Selected Topic in Applied Earth Observations and Remote Sensing*. He is a Member of IEEE.

REFERENCES

- [1] J.-s Zhang, C.-y He, Y.-z Pan, and J. Li, "The high spatial resolution RS image classification based on SVM method with the multi-source data," *J. Remote Sens.-Beijing*, vol. 10, no. 1, pp. 49, 2006.
- [2] W. Zhao, S. Du, Q. Wang, and W. J. Emery, "Contextually guided very-high-resolution imagery classification with semantic segments," *ISPRS J. Photogrammetry Remote Sens.*, vol. 132, pp. 48–60, Oct. 2017. doi: 10.1016/j.isprsjprs.2017.08.011.
- [3] N. Longbotham, C. Chaapel, L. Bleiler, C. Padwick, W. J. Emery, and F. Pacifici, "Very high resolution multiangle urban classification analysis," *IEEE Trans. Geosci. Remote Sens.*, vol. 50, no. 4, pp. 1155–1170, 2011. doi: 10.1109/TGRS.2011.2165548.
- [4] J. C.-W. Chan, R. Bellens, F. Canters, and S. Gautama, "An assessment of geometric activity features for per-pixel classification of urban man-made objects using very high resolution satellite imagery," *Photogrammetric Eng. Remote Sens.*, vol. 75, no. 4, pp. 397–411, 2009. doi: 10.14358/PERS.75.4.397.
- [5] F. Pacifici, M. Chini, and W. J. Emery, "A neural network approach using multi-scale textural metrics from very high-resolution panchromatic imagery for urban land-use classification," *Remote Sens. Environ.*, vol. 113, no. 6, pp. 1276–1292, 2009. doi: 10.1016/j.rse.2009.02.014.
- [6] X. Huang, L. Zhang, and P. Li, "An adaptive multiscale information fusion approach for feature extraction and classification of IKONOS multispectral imagery over urban areas," *IEEE Geosci. Remote Sens. Lett.*, vol. 4, no. 4, pp. 654–658, 2007. doi: 10.1109/LGRS.2007.905121.
- [7] X. Huang, L. Zhang, and P. Li, "A multiscale feature fusion approach for classification of very high resolution satellite imagery based on wavelet transform," *Int. J. Remote Sens.*, vol. 29, no. 20, pp. 5923–5941, 2008. doi: 10.1080/01431160802139922.
- [8] N. Mitraklis, C. Topaloglou, T. Alexandridis, J. Theocaris, and G. Zalidis, "A novel self-organizing neuro-fuzzy multilayered classifier for land cover classification of a VHR image," *Int. J. Remote Sens.*, vol. 29, no. 14, pp. 4061–4087, 2008. doi: 10.1080/01431160801891846.
- [9] B. Demir and L. Bruzzone, "Histogram-based attribute profiles for classification of very high resolution remote sensing images," *IEEE Trans. Geosci. Remote Sens.*, vol. 54, no. 4, pp. 2096–2107, 2015. doi: 10.1109/TGRS.2015.2496167.
- [10] C. Huo, Z. Zhou, H. Lu, C. Pan, and K. Chen, "Fast object-level change detection for VHR images," *IEEE Geosci. Remote Sens. Lett.*, vol. 7, no. 1, pp. 118–122, 2009. doi: 10.1109/LGRS.2009.2028438.
- [11] M. Li, S. Zang, B. Zhang, S. Li, and C. Wu, "A review of remote sensing image classification techniques: The role of spatio-contextual information," *Eur. J. Remote Sen.*, vol. 47, no. 1, pp. 389–411, 2014. doi: 10.5721/EuJRS20144723.
- [12] B. Salehi, Y. Ming Zhong, and V. Dey, "A review of the effectiveness of spatial information used in urban land cover classification of VHR imagery," *Int. J. Geoinf.*, vol. 8, no. 2, p. 35, 2012.
- [13] S. Chaib, H. Liu, Y. Gu, and H. Yao, "Deep feature fusion for VHR remote sensing scene classification," *IEEE Trans. Geosci. Remote Sens.*, vol. 55, no. 8, pp. 4775–4784, 2017. doi: 10.1109/TGRS.2017.2700322.
- [14] Q. Wang, S. Liu, J. Chanussot, and X. Li, "Scene classification with recurrent attention of VHR remote sensing images," *IEEE Trans. Geosci. Remote Sens.*, vol. 57, no. 2, pp. 1155–1167, 2018. doi: 10.1109/TGRS.2018.2864987.
- [15] G. Cheng, J. Han, L. Guo, Z. Liu, S. Bu, and J. Ren, "Effective and efficient midlevel visual elements-oriented land-use classification using VHR remote sensing images," *IEEE Trans. Geosci. Remote Sens.*, vol. 53, no. 8, pp. 4238–4249, 2015. doi: 10.1109/TGRS.2015.2393857.
- [16] T. Peng, I. H. Jermyn, V. Prinet, and J. Zerubia, "Incorporating generic and specific prior knowledge in a multiscale phase field model for road extraction from VHR images," *IEEE J. Sel. Topics Appl. Earth Observ. Remote Sens.*, vol. 1, no. 2, pp. 139–146, 2008. doi: 10.1109/JSTARS.2008.922318.
- [17] H. Liu, M. Yang, J. Chen, J. Hou, and M. Deng, "Line-constrained shape feature for building change detection in VHR remote sensing imagery," *ISPRS Int. J. Geo-Inform.*, vol. 7, no. 10, p. 410, 2018. doi: 10.3390/ijgi7100410.
- [18] N. Falco, M. Dalla Mura, F. Bovolo, J. A. Benediktsson, and L. Bruzzone, "Change detection in VHR images based on morphological attribute profiles," *IEEE Geosci. Remote Sens. Lett.*, vol. 10, no. 3, pp. 636–640, 2012. doi: 10.1109/LGRS.2012.2222340.
- [19] D. Arvor, L. Durieux, S. Andrs, and M.-A. Laporte, "Advances in geographic object-based image analysis with ontologies: A review of main contributions and limitations from a remote sensing perspective," *ISPRS J. Photogrammetry Remote Sens.*, vol. 82, pp. 125–137, Aug. 2013. doi: 10.1016/j.isprsjprs.2013.05.003.
- [20] P. C. Smits and A. Annoni, "Updating land-cover maps by using texture information from very high-resolution space-borne imagery," *IEEE Trans. Geosci. Remote Sens.*, vol. 37, no. 3, pp. 1244–1254, 1999. doi: 10.1109/36.763282.
- [21] P. J. Li, H. Q. Xu, and J. C. Guo, "Urban building damage detection from very high resolution imagery using OCSVM and spatial features," *Int. J. Remote Sens.*, vol. 31, no. 13, pp. 3393–3409, 2010. doi: 10.1080/01431161003727705.

- [22] P. Li, B. Song, and H. Xu, "Urban building damage detection from very high resolution imagery by one-class SVM and shadow information," in *Proc. 2011 IEEE Int. Geosci. Remote Sens. Symp.*, pp. 1409–1412. doi: 10.1109/IGARSS.2011.6049330.
- [23] R. Anniballe et al., "Earthquake damage mapping: An overall assessment of ground surveys and VHR image change detection after L'Aquila 2009 earthquake," *Remote Sens. Environ.*, vol. 210, pp. 166–178, June 2018. doi: 10.1016/j.rse.2018.03.004.
- [24] P. Gong, E. LeDrew, and J. Miller, "Registration-noise reduction in difference images for change detection," *Int. J. Remote Sens.*, vol. 13, no. 4, pp. 773–779, 1992. doi: 10.1080/01431169208904151.
- [25] Y. Han, F. Bovolo, and L. Bruzzone, "An approach to fine coregistration between very high resolution multispectral images based on registration noise distribution," *IEEE Trans. Geosci. Remote Sens.*, vol. 53, no. 12, pp. 6650–6662, 2015. doi: 10.1109/TGRS.2015.2445632.
- [26] S. Marchesi, F. Bovolo, and L. Bruzzone, "A context-sensitive technique robust to registration noise for change detection in VHR multispectral images," *IEEE Trans. Image Process.*, vol. 19, no. 7, pp. 1877–1889, 2010. doi: 10.1109/TIP.2010.2045070.
- [27] F. Bovolo, L. Bruzzone, and S. Marchesi, "Analysis and adaptive estimation of the registration noise distribution in multitemporal VHR images," *IEEE Trans. Geosci. Remote Sens.*, vol. 47, no. 8, pp. 2658–2671, 2009. doi: 10.1109/TGRS.2009.2017014.
- [28] Y. Han, F. Bovolo, and L. Bruzzone, "Edge-based registration-noise estimation in VHR multitemporal and multisensor images," *IEEE Geosci. Remote Sens. Lett.*, vol. 13, no. 9, pp. 1231–1235, 2016. doi: 10.1109/LGRS.2016.2577719.
- [29] N. Falco, P. R. Marpu, and J. A. Benediktsson, "A toolbox for unsupervised change detection analysis," *Int. J. Remote Sens.*, vol. 37, no. 7, pp. 1505–1526, 2016. doi: 10.1080/01431161.2016.1154226.
- [30] L. Bruzzone, F. Bovolo, and S. Marchesi, "A multiscale change detection technique robust to registration noise," in *Proc. Int. Conf. Pattern Recognit. Mach. Intell.*, Springer, 2007, pp. 77–86. doi: 10.1007/978-3-540-77046-6_10.
- [31] X. Zhu, H. Cao, Y. Zhang, K. Tan, and X. Ling, "Fine registration for VHR images based on superpixel registration-noise estimation," *IEEE Geosci. Remote Sens. Lett.*, vol. 15, no. 10, pp. 1615–1619, 2018. doi: 10.1109/LGRS.2018.2849696.
- [32] Z. Li, W. Shi, S. W. Myint, P. Lu, and Q. Wang, "Semi-automated landslide inventory mapping from bitemporal aerial photographs using change detection and level set method," *Remote Sens. Environ.*, vol. 175, pp. 215–230, Mar. 2016. doi: 10.1016/j.rse.2016.01.003.
- [33] Y. Ban and O. Yousif, *Change Detection Techniques: A Review*. New York: Springer-Verlag, 2016, pp. 19–43.
- [34] L. Bruzzone and F. Bovolo, "A novel framework for the design of change-detection systems for very-high-resolution remote sensing images," *Proc. IEEE*, vol. 101, no. 3, pp. 609–630, 2012. doi: 10.1109/JPROC.2012.2197169.
- [35] M. Dalla Mura, J. A. Benediktsson, F. Bovolo, and L. Bruzzone, "An unsupervised technique based on morphological filters for change detection in very high resolution images," *IEEE Geosci. Remote Sens. Lett.*, vol. 5, no. 3, pp. 433–437, 2008. doi: 10.1109/LGRS.2008.917726.
- [36] I. Niemeyer, P. R. Marpu, and S. Nussbaum, *Change Detection using Object Features*. New York: Springer-Verlag, 2008, pp. 185–201.
- [37] H. Zhang, J. Chen, and Z. Mao, "The research on relative radiometric normalization for change detection of multitemporal images," in *Proc. Conf. Image Signal Process. Remote Sens. XV*, vol. 7477, p. 747.714. doi: 10.1117/12.830199.
- [38] M. Hao, H. Zhang, W. Shi, and K. Deng, "Unsupervised change detection using fuzzy c-means and MRF from remotely sensed images," *Remote Sens. Lett.*, vol. 4, no. 12, pp. 1185–1194, 2013. doi: 10.1080/2150704X.2013.858841.
- [39] W. Zhao, L. Mou, J. Chen, Y. Bo, and W. J. Emery, "Incorporating metric learning and adversarial network for seasonal invariant change detection," *IEEE Trans. Geosci. Remote Sens.*, vol. 58, no. 4, pp. 2720–2731, 2019. doi: 10.1109/TGRS.2019.2953879.
- [40] L. He, J. Li, C. Liu, and S. Li, "Recent advances on spectral-spatial hyperspectral image classification: An overview and new guidelines," *IEEE Trans. Geosci. Remote Sens.*, vol. 56, no. 3, pp. 1579–1597, 2017. doi: 10.1109/TGRS.2017.2765364.
- [41] S. Liu, D. Marinelli, L. Bruzzone, and F. Bovolo, "A review of change detection in multitemporal hyperspectral images: Current techniques, applications, and challenges," *IEEE Geosci. Remote Sens. Mag. (replaces Newslett.)*, vol. 7, no. 2, pp. 140–158, 2019. doi: 10.1109/MGRS.2019.2898520.
- [42] P. Coppin, I. Jonckheere, K. Nackaerts, B. Muys, and E. Lambin, "Review articledigital change detection methods in ecosystem monitoring: Review," *Int. J. Remote Sens.*, vol. 25, no. 9, pp. 1565–1596, 2004. doi: 10.1080/0143116031000101675.
- [43] S. Yadav, I. Rizvi, and S. Kadam, "Urban tree canopy detection using object-based image analysis for very high resolution satellite images: A literature review," in *Proc. 2015 Int. Conf. Technol. Sustain. Develop.*, pp. 1–6. doi: 10.1109/ICTSD.2015.7095889.
- [44] C. Benedek and T. Szirnyi, "Change detection in optical aerial images by a multilayer conditional mixed Markov model," *IEEE Trans. Geosci. Remote Sens.*, vol. 47, no. 10, pp. 3416–3430, 2009. doi: 10.1109/TGRS.2009.2022633.
- [45] F. Bovolo and L. Bruzzone, "The time variable in data fusion: A change detection perspective," *IEEE Geosci. Remote Sens. Mag. (replaces Newslett.)*, vol. 3, no. 3, pp. 8–26, 2015. doi: 10.1109/MGRS.2015.2443494.
- [46] C. Benedek, M. Shadaydeh, Z. Kato, T. Szirnyi, and J. Zerubia, "Multilayer Markov random field models for change detection in optical remote sensing images," *ISPRS J. Photogrammetry Remote Sens.*, vol. 107, pp. 22–37, Sept. 2015. doi: 10.1016/j.isprsjprs.2015.02.006.
- [47] Z. F. Zheng, J. N. Cao, Z. Y. Lv, and J. A. Benediktsson, "Spatial-spectral feature fusion coupled with multi-scale segmentation voting decision for detecting land cover change with VHR remote sensing images," *Remote Sens.*, vol. 11, no. 16, pp. 22–37, 2019. doi: 10.3390/rs11161903.
- [48] C. T. Wei, P. Zhao, X. Y. Li, Y. B. Wang, and F. Y. Liu, "Unsupervised change detection of VHR remote sensing images based on multi-resolution Markov random field in wavelet domain," *Int. J. Remote Sens.*, vol. 40, no. 20, pp. 7750–7766, 2019. doi: 10.1080/01431161.2019.1602792.

- [49] L. Zhou, G. Cao, Y. Li, and Y. Shang, "Change detection based on conditional random field with region connection constraints in high-resolution remote sensing images," *IEEE J. Sel. Topics Appl. Earth Observ. Remote Sens.*, vol. 9, no. 8, pp. 3478–3488, 2016. doi: 10.1109/JSTARS.2016.2514610.
- [50] Z. Li, W. Shi, H. Zhang, and M. Hao, "Change detection based on Gabor wavelet features for very high resolution remote sensing images," *IEEE Geosci. Remote Sens. Lett.*, vol. 14, no. 5, pp. 783–787, 2017. doi: 10.1109/LGRS.2017.2681198.
- [51] M. Janalipour and M. Taleai, "Building change detection after earthquake using multi-criteria decision analysis based on extracted information from high spatial resolution satellite images," *Int. J. Remote Sens.*, vol. 38, no. 1, pp. 82–99, 2017. doi: 10.1080/01431161.2016.1259673.
- [52] Y. Xu, C. L. Huo, S. M. Xiang, and C. H. Pan, "Robust VHR image change detection based on local features and multi-scale fusion," in *Proc. Int. Conf. Acoustics Speech Signal Process. (ICASSP)*, 2013, pp. 1991–1995. doi: 10.1109/ICASSP.2013.6638002.
- [53] H. Chen, C. Wu, B. Du, and L. Zhang, "Deep Siamese multi-scale convolutional network for change detection in multitemporal VHR images," in *Proc. 2019 10th Int. Workshop on Analysis Multitemporal Remote Sens. Images (MultiTemp)*, pp. 1–4. doi: 10.1109/Multi-Temp.2019.8866947.
- [54] D. F. Peng and Y. J. Zhang, "Object-based change detection method using refined Markov random field," *J. Appl. Remote Sens.*, vol. 11, no. 1, p. 016024, 2017. doi: 10.1117/1.JRS.11.016024.
- [55] Z. Y. Lv, T. F. Liu, J. A. Benediktsson, T. Lei, and Y. L. Wan, "Multi-scale object histogram distance for LCCD using bi-temporal very-high-resolution remote sensing images," *Remote Sens.*, vol. 10, no. 11, p. 1809, 2018. doi: 10.3390/rs10111809.
- [56] Y. Zhang, D. Peng, and X. Huang, "Object-based change detection for VHR images based on multiscale uncertainty analysis," *IEEE Geosci. Remote Sens. Lett.*, vol. 15, no. 1, pp. 13–17, 2017. doi: 10.1109/LGRS.2017.2763182.
- [57] P. F. Xiao, M. Yuan, X. L. Zhang, X. Z. Feng, and Y. W. Guo, "Cosegmentation for object-based building change detection from high-resolution remotely sensed images," *IEEE Trans. Geosci. Remote Sens.*, vol. 55, no. 3, pp. 1587–1603, 2017. doi: 10.1109/TGRS.2016.2627638.
- [58] J. L. Gil-Yepes, L. A. Ruiz, J. A. Recio, A. Balaguer-Beser, and T. Hermosilla, "Description and validation of a new set of object-based temporal geostatistical features for land-use/land-cover change detection," *ISPRS J. Photogrammetry Remote Sens.*, vol. 121, pp. 77–91, Nov. 2016. doi: 10.1016/j.isprsjprs.2016.08.010.
- [59] M. Hussain, D. Chen, A. Cheng, H. Wei, and D. Stanley, "Change detection from remotely sensed images: From pixel-based to object-based approaches," *ISPRS J. Photogrammetry Remote Sens.*, vol. 80, pp. 91–106, June 2013. doi: 10.1016/j.isprsjprs.2013.03.006.
- [60] Y. Kosugi, M. Sakamoto, M. Fukunishi, W. Lu, T. Doihara, and S. Kakumoto, "Urban change detection related to earthquakes using an adaptive nonlinear mapping of high-resolution images," *IEEE Geosci. Remote Sens. Lett.*, vol. 1, no. 3, pp. 152–156, 2004. doi: 10.1109/LGRS.2004.828917.
- [61] F. Bovolo, L. Bruzzone, and S. Marchesi, "An adaptive parcel-based technique robust to registration noise for change detection in multitemporal VHR images," in *Proc. Soc. Photo-Optical Instrumentation Eng. (SPIE)*, 2007, vol. 6748, pp. 674,806. doi: 10.1117/12.739223.
- [62] X. Gong and T. Corpetti, "Adaptive window size estimation in unsupervised change detection," *IEEE J. Sel. Topics Appl. Earth Observ. Remote Sens.*, vol. 6, no. 2, pp. 991–1003, 2012. doi: 10.1109/JSTARS.2012.2220531.
- [63] Z. Y. Lv, T. F. Liu, P. L. Zhang, J. A. Benediktsson, T. Lei, and X. K. Zhang, "Novel adaptive histogram trend similarity approach for land cover change detection by using bitemporal very-high-resolution remote sensing images," *IEEE Trans. Geosci. Remote Sens.*, vol. 57, no. 12, pp. 9554–9574, 2019. doi: 10.1109/TGRS.2019.2927659.
- [64] Y. T. Solano-Correa, F. Bovolo, and L. Bruzzone, "An approach to multiple change detection in VHR optical images based on iterative clustering and adaptive thresholding," *IEEE Geosci. Remote Sens. Lett.*, vol. 16, no. 8, pp. 1334–1338, 2019. doi: 10.1109/LGRS.2019.2896385.
- [65] A. Radoi and M. Datcu, "Automatic change analysis in satellite images using binary descriptors and lloyd–max quantization," *IEEE Geosci. Remote Sens. Lett.*, vol. 12, no. 6, pp. 1223–1227, 2015. doi: 10.1109/LGRS.2015.2389144.
- [66] N. Champion, D. Boldo, M. Pierrot-Deseilligny, and G. Stamon, "2d building change detection from high resolution satellite imagery: A two-step hierarchical method based on 3d invariant primitives," *Pattern Recognit. Lett.*, vol. 31, no. 10, pp. 1138–1147, 2010. doi: 10.1016/j.patrec.2009.10.012.
- [67] Y. Tang, X. Huang, and L. Zhang, "Fault-tolerant building change detection from urban high-resolution remote sensing imagery," *IEEE Geosci. Remote Sens. Lett.*, vol. 10, no. 5, pp. 1060–1064, 2013. doi: 10.1109/LGRS.2012.2228626.
- [68] H. Sui, D. Li, and J. Gong, "Automatic feature-level change detection (FLCD) for road networks," *Int. Soc. Photogramm. Remote Sens. Geo-Imag. Bridg. Cont.*, pp. 459–464, 2004.
- [69] P. Zhang, Z. Lv, and W. Shi, "Local spectrum-trend similarity approach for detecting land-cover change by using spot-5 satellite images," *IEEE Geosci. Remote Sens. Lett.*, vol. 11, no. 4, pp. 738–742, 2013. doi: 10.1109/LGRS.2013.2278205.
- [70] M. Aktar, M. Mamun, and M. Hossain, "Statistical similarity based change detection for multitemporal remote sensing images," *J. Elect. Comput. Eng.*, vol. 2017, 2017. doi: 10.1155/2017/3123967.
- [71] M. Volpi, D. Tuia, F. Bovolo, M. Kanevski, and L. Bruzzone, "Supervised change detection in VHR images using contextual information and support vector machines," *Int. J. Appl. Earth Observ. Geoinf.*, vol. 20, pp. 77–85, Feb. 2013. doi: 10.1016/j.jag.2011.10.013.
- [72] J. Chen, H. Liu, J. Hou, M. Yang, and M. Deng, "Improving building change detection in vhr remote sensing imagery by combining coarse location and co-segmentation," *ISPRS Int. J. Geo-Inform.*, vol. 7, no. 6, p. 213, 2018. doi: 10.3390/ijgi7060213.
- [73] M. Volpi, D. Tuia, M. Kanevski, F. Bovolo, and L. Bruzzone, "Supervised change detection in VHR images: A comparative analysis," in *Proc. 2009 IEEE Int. Workshop on Mach. Learn. Signal Process.*, pp. 1–6. doi: 10.1109/MLSP.2009.5306259.
- [74] P. Xiao, X. Zhang, D. Wang, M. Yuan, X. Feng, and M. Kelly, "Change detection of built-up land: A framework of combining

- pixel-based detection and object-based recognition," *ISPRS J. Photogrammetry Remote Sens.*, vol. 119, pp. 402–414, Sept. 2016. doi: 10.1016/j.isprsjprs.2016.07.003.
- [75] B. Wu et al., "Parcel-based change detection in land-use maps by adopting the holistic feature," *IEEE J. Sel. Topics Appl. Earth Observ. Remote Sens.*, vol. 7, no. 8, pp. 3482–3490, 2014. doi: 10.1109/JSTARS.2013.2291773.
- [76] S. Hong and R. R. Vatsavai, "Sliding window-based probabilistic change detection for remote-sensed images," *Procedia Comput. Sci.*, vol. 80, pp. 2348–2352, June 2016. doi: 10.1016/j.procs.2016.05.438.
- [77] S. Liu, Q. Du, X. Tong, A. Samat, L. Bruzzone, and F. Bovolo, "Multiscale morphological compressed change vector analysis for unsupervised multiple change detection," *IEEE J. Sel. Topics Appl. Earth Observ. Remote Sens.*, vol. 10, no. 9, pp. 4124–4137, 2017. doi: 10.1109/JSTARS.2017.2712119.
- [78] N. Falco, M. Dalla Mura, F. Bovolo, J. A. Benediktsson, and L. Bruzzone, "Study on the capabilities of morphological attribute profiles in change detection on VHR images," in *Proc. SPIE*, 2010, vol. 7830, p. 783,016. doi: 10.1117/12.866178.
- [79] X. Huang, L. P. Zhang, and T. T. Zhu, "Building change detection from multitemporal high-resolution remotely sensed images based on a morphological building index," *IEEE J. Sel. Topics Appl. Earth Observ. Remote Sens.*, vol. 7, no. 1, pp. 105–115, 2014. doi: 10.1109/JSTARS.2013.2252423.
- [80] J. Liu, M. Gong, K. Qin, and P. Zhang, "A deep convolutional coupling network for change detection based on heterogeneous optical and radar images," *IEEE Trans. Neural Netw. Learn. Syst.*, vol. 29, no. 3, pp. 545–559, 2016. doi: 10.1109/TNNLS.2016.2636227.
- [81] F. Pacifici and F. Del Frate, "Automatic change detection in very high resolution images with pulse-coupled neural networks," *IEEE Geosci. Remote Sens. Lett.*, vol. 7, no. 1, pp. 58–62, 2010. doi: 10.1109/LGRS.2009.2021780.
- [82] Y. Wang, B. Du, L. Ru, C. Wu, and H. Luo, "Scene change detection via deep convolution canonical correlation analysis neural network," in *Proc. IGARSS 2019 IEEE Int. Geosci. Remote Sens. Symp.*, pp. 198–201. doi: 10.1109/IGARSS.2019.8898211.
- [83] S. Ji, Y. Shen, M. Lu, and Y. Zhang, "Building instance change detection from large-scale aerial images using convolutional neural networks and simulated samples," *Remote Sens.*, vol. 11, no. 11, p. 1343, 2019. doi: 10.3390/rs1111343.
- [84] H. Chen, C. Wu, B. Du, L. Zhang, and L. Wang, "Change detection in multisource VHR images via deep Siamese convolutional multiple-layers recurrent neural network," *IEEE Trans. Geosci. Remote Sens.*, vol. 58, no. 4, pp. 2848–2864, 2019. doi: 10.1109/TGRS.2019.2956756.
- [85] H. Zhang, M. G. Gong, P. Z. Zhang, L. Z. Su, and J. Shi, "Feature-level change detection using deep representation and feature change analysis for multispectral imagery," *IEEE Geosci. Remote Sens. Lett.*, vol. 13, no. 11, pp. 1666–1670, 2016. doi: 10.1109/LGRS.2016.2601930.
- [86] X. D. Niu, M. G. Gong, T. Zhan, and Y. L. Yang, "A conditional adversarial network for change detection in heterogeneous images," *IEEE Geosci. Remote Sens. Lett.*, vol. 16, no. 1, pp. 45–49, 2019. doi: 10.1109/LGRS.2018.2868704.
- [87] Q. M. Wang, W. Z. Shi, P. M. Atkinson, and Z. B. Li, "Land cover change detection at subpixel resolution with a Hopfield neural network," *IEEE J. Sel. Topics Appl. Earth Observ. Remote Sens.*, vol. 8, no. 3, pp. 1339–1352, 2015. doi: 10.1109/JSTARS.2014.2355832.
- [88] D. F. Peng, Y. J. Zhang, and H. Y. Guan, "End-to-end change detection for high resolution satellite images using improved UNet plus," *Remote Sens.*, vol. 11, no. 11, p. 23, 2019. doi: 10.3390/rs11111382.
- [89] S. Saha, F. Bovolo, and L. Bruzzone, "Unsupervised deep change vector analysis for multiple-change detection in VHR images," *IEEE Trans. Geosci. Remote Sens.*, vol. 57, no. 6, pp. 3677–3693, 2019. doi: 10.1109/TGRS.2018.2886643.
- [90] Y. Zhong, W. Liu, J. Zhao, and L. Zhang, "Change detection based on pulse-coupled neural networks and the NMI feature for high spatial resolution remote sensing imagery," *IEEE Geosci. Remote Sens. Lett.*, vol. 12, no. 3, pp. 537–541, 2014. doi: 10.1109/LGRS.2014.2349937.
- [91] H. Yu, W. Yang, G. Hua, H. Ru, and P. P. Huang, "Change detection using high resolution remote sensing images based on active learning and Markov random fields," *Remote Sens.*, vol. 9, no. 12, p. 21, 2017. doi: 10.3390/rs9121233.
- [92] B. Belmudez, V. Prinet, J.-F. Yao, P. Bouthemy, and X. Descombes, "Conditional mixed-state model for structural change analysis from very high resolution optical images," in *Proc. IEEE Int. Symp. Geosci. Remote Sens. (IGARSS)*, 2009, p. 1239. doi: 10.1109/IGARSS.2009.5418267.
- [93] G. Cao, L. Zhou, and Y. Li, "A new change-detection method in high-resolution remote sensing images based on a conditional random field model," *Int. J. Remote Sens.*, vol. 37, no. 5, pp. 1173–1189, 2016. doi: 10.1080/01431161.2016.1148284.
- [94] P. Y. Lv, Y. F. Zhong, J. Zhao, H. Z. Jiao, and L. P. Zhang, "Change detection based on a multifeature probabilistic ensemble conditional random field model for high spatial resolution remote sensing imagery," *IEEE Geosci. Remote Sens. Lett.*, vol. 13, no. 12, pp. 1965–1969, 2016. doi: 10.1109/LGRS.2016.2619163.
- [95] P. Lv, Y. Zhong, J. Zhao, and L. Zhang, "Unsupervised change detection based on hybrid conditional random field model for high spatial resolution remote sensing imagery," *IEEE Trans. Geosci. Remote Sens.*, vol. 56, no. 7, pp. 4002–4015, 2018. doi: 10.1109/TGRS.2018.2819367.
- [96] M. Hao, W. Z. Shi, H. Zhang, and C. Li, "Unsupervised change detection with expectation-maximization-based level set," *IEEE Geosci. Remote Sens. Lett.*, vol. 11, no. 1, pp. 210–214, 2014. doi: 10.1109/LGRS.2013.2252879.
- [97] G. Cao, Y. Z. Liu, and Y. F. Shang, "Automatic change detection in remote sensing images using level set method with neighborhood constraints," *J. Appl. Remote Sens.*, vol. 8, no. 1, p. 083678, 2014. doi: 10.1117/1.JRS.8.083678.
- [98] H. S. Zhang, J. Y. Chen, and X. Liu, "Object-based change detection on multiscale fusion for VHR remote sensing images," in *Proc. SPIE*, 2015, vol. 9815, p. 98150L. doi: 10.1117/12.2205593.
- [99] C. Shi, Z. Lv, H. Shen, L. Fang, and Z. You, "Improved metric learning with the CNN for very-high-resolution remote sensing image classification," *IEEE J. Sel. Topics Appl. Earth Observ.*

- Remote Sens.*, vol. 14, no. 6, pp. 631–644, 2021. doi: 10.1109/JSTARS.2020.3033944.
- [100] K. Ding, C. Huo, Y. Xu, Z. Zhong, and C. Pan, “Sparse hierarchical clustering for VHR image change detection,” *IEEE Geosci. Remote Sens. Lett.*, vol. 12, no. 3, pp. 577–581, 2014. doi: 10.1109/LGRS.2014.2351807.
- [101] T. Blaschke, “Object based image analysis for remote sensing,” *ISPRS J. Photogrammetry Remote Sens.*, vol. 65, no. 1, pp. 2–16, 2010. doi: 10.1016/j.isprsjprs.2009.06.004.
- [102] T. Blaschke et al., “Geographic object-based image analysis—towards a new paradigm,” *ISPRS J. Photogrammetry Remote Sens.*, vol. 87, pp. 180–191, Jan. 2014. doi: 10.1016/j.isprsjprs.2013.09.014.
- [103] J. Chen, Z. Mao, B. Philpot, J. Li, and D. Pan, “Detecting changes in high-resolution satellite coastal imagery using an image object detection approach,” *Int. J. Remote Sens.*, vol. 34, no. 7, pp. 2454–2469, 2013. doi: 10.1080/01431161.2012.743691.
- [104] Q. Chen, Y. H. Chen, and W. G. Jiang, “Genetic particle swarm optimization based feature selection for very-high-resolution remotely sensed imagery object change detection,” *Sensors*, vol. 16, no. 8, p. 20, 2016. doi: 10.3390/s16081204.
- [105] M. Hao, W. Z. Shi, K. H. Deng, H. Zhang, and P. F. He, “An object-based change detection approach using uncertainty analysis for VHR images,” *J. Sens.*, vol. 2016, p. 9,078,364, 2016. doi: 10.1155/2016/9078364.
- [106] J. Im, J. Jensen, and J. Tullis, “Objectbased change detection using correlation image analysis and image segmentation,” *Int. J. Remote Sens.*, vol. 29, no. 2, pp. 399–423, 2008. doi: 10.1080/01431160601075582.
- [107] C. Listner and I. Niemeyer, “Object-based change detection,” *Photogrammetrie-Fernerkundung-Geoinf.*, vol. 2011, no. 4, pp. 233–245, 2011. doi: 10.1127/1432-8364/2011/0085.
- [108] Z. Hu, Q. Zhang, Q. Zou, Q. Li, and G. Wu, “Stepwise evolution analysis of the region-merging segmentation for scale parameterization,” *IEEE J. Sel. Topics Appl. Earth Observ. Remote Sens.*, vol. 11, no. 7, pp. 2461–2472, 2018. doi: 10.1109/JSTARS.2018.2833102.
- [109] J. Aguirre-Gutierrez, A. C. Seijmonsbergen, and J. F. Duivenvoorden, “Optimizing land cover classification accuracy for change detection, a combined pixel-based and object-based approach in a mountainous area in Mexico,” *Appl. Geograph.*, vol. 34, pp. 29–37, May 2012. doi: 10.1016/j.apgeog.2011.10.010.
- [110] Z. J. Zhou, L. Ma, T. Y. Fu, G. Zhang, M. R. Yao, and M. C. Li, “Change detection in coral reef environment using high-resolution images: Comparison of object-based and pixel-based paradigms,” *ISPRS Int. J. Geo-Inf.*, vol. 7, no. 11, p. 27, 2018. doi: 10.3390/ijgi7110441.
- [111] H. Nemmour and Y. Chibani, “Fuzzy neural network architecture for change detection in remotely sensed imagery,” *Int. J. Remote Sens.*, vol. 27, no. 4, pp. 705–717, 2006. doi: 10.1080/01431160500275648.
- [112] D. Peng, Y. Zhang, and H. Guan, “End-to-end change detection for high resolution satellite images using improved UNet+,” *Remote Sens.*, vol. 11, no. 11, p. 1382, 2019. doi: 10.3390/rs11111382.
- [113] A. Karpatne, Z. Jiang, R. R. Vatsavai, S. Shekhar, and V. Kumar, “Monitoring land-cover changes: A machine-learning perspective,” *IEEE Geosci. Remote Sens. Mag. (replaces Newslett.)*, vol. 4, no. 2, pp. 8–21, 2016. doi: 10.1109/MGRS.2016.2528038.
- [114] S. Liu, L. Bruzzone, F. Bovolo, and P. Du, “Hierarchical unsupervised change detection in multitemporal hyperspectral images,” *IEEE Trans. Geosci. Remote Sens.*, vol. 53, no. 1, pp. 244–260, 2014. doi: 10.1109/TGRS.2014.2321277.
- [115] F. Bovolo, “A multilevel parcel-based approach to change detection in very high resolution multitemporal images,” *IEEE Geosci. Remote Sens. Lett.*, vol. 6, no. 1, pp. 33–37, 2008. doi: 10.1109/LGRS.2008.2007429.
- [116] Z. Y. Lv, W. Shi, X. Zhang, and J. A. Benediktsson, “Landslide inventory mapping from bitemporal high-resolution remote sensing images using change detection and multi-scale segmentation,” *IEEE J. Sel. Topics Appl. Earth Observ. Remote Sens.*, vol. 11, no. 5, pp. 1520–1532, 2018. doi: 10.1109/JSTARS.2018.2803784.
- [117] Z. Lv, T. Liu, C. Shi, J. A. Benediktsson, and H. Du, “Novel land cover change detection method based on k-means clustering and adaptive majority voting using bitemporal remote sensing images,” *IEEE Access*, vol. 7, pp. 34,425–34,437, Jan. 2019. doi: 10.1109/ACCESS.2019.2892648.
- [118] M. Vakalopoulou, K. Karantzalos, N. Komodakis, and N. Paragios, “Simultaneous registration and change detection in multitemporal, very high resolution remote sensing data,” in *Proc. IEEE Conf. Comput. Vis. Pattern Recognit. (CVPR) Workshops*, 2015, pp. 61–69.
- [119] C. Wu, L. Zhang, and L. Zhang, “A scene change detection framework for multi-temporal very high resolution remote sensing images,” *Signal Process.*, vol. 124, pp. 184–197, July 2016. doi: 10.1016/j.sigpro.2015.09.020.
- [120] C. Wu, L. Zhang, and B. Du, “Kernel slow feature analysis for scene change detection,” *IEEE Trans. Geosci. Remote Sens.*, vol. 55, no. 4, pp. 2367–2384, 2017. doi: 10.1109/TGRS.2016.2642125.
- [121] J. Tu, D. Li, W. Feng, Q. Han, and H. Sui, “Detecting damaged building regions based on semantic scene change from multitemporal high-resolution remote sensing images,” *ISPRS Int. J. Geo-Inf.*, vol. 6, no. 5, p. 131, 2017. doi: 10.3390/ijgi6050131.
- [122] B. Chen, Z. Chen, L. Deng, Y. Duan, and J. Zhou, “Building change detection with RGB-d map generated from UAV images,” *Neurocomputing*, vol. 208, pp. 350–364, Oct. 2016. doi: 10.1016/j.neucom.2015.11.118.
- [123] C. Stal, F. Tack, P. De Maeyer, A. De Wulf, and R. Goossens, “Airborne photogrammetry and lidar for DSM extraction and 3d change detection over an urban area—a comparative study,” *Int. J. Remote Sens.*, vol. 34, no. 4, pp. 1087–1110, 2013. doi: 10.1080/01431161.2012.717183.
- [124] I. Eden and D. B. Cooper, “Using 3d line segments for robust and efficient change detection from multiple noisy images,” in *Proc. Eur. Conf. Comput. Vis.*, pp. 172–185, 2008. doi: 10.1007/978-3-540-88693-8_13.
- [125] J. Tian, S. Cui, and P. Reinartz, “Building change detection based on satellite stereo imagery and digital surface models,” *IEEE Trans. Geosci. Remote Sens.*, vol. 52, no. 1, pp. 406–417, 2013. doi: 10.1109/TGRS.2013.2240692.
- [126] J. Tian, H. Chaabouni-Chouayakh, and P. Reinartz, “3d building change detection from high resolution spaceborne

- stereo imagery," in *Proc. Int. Workshop on Multi-Platform/Multi-Sensor Remote Sens. Mapping*, 2011, pp. 1–7. doi: 10.1109/M2RSM.2011.5697371.
- [127] R. Qin, J. Tian, and P. Reinartz, "3d change detection-approaches and applications," *ISPRS J. Photogrammetry Remote Sens.*, vol. 122, pp. 41–56, Dec. 2016. doi: 10.1016/j.isprsjprs.2016.09.013.
- [128] G. Liu, Y. Gousseau, and F. Tupin, "A Contrario comparison of local descriptors for change detection in very high spatial resolution satellite images of urban areas," *IEEE Trans. Geosci. Remote Sens.*, vol. 57, no. 6, pp. 3904–3918, 2019. doi: 10.1109/TGRS.2018.2888985.
- [129] C. Marin, F. Bovolo, and L. Bruzzone, "Building change detection in multitemporal very high resolution Sar images," *IEEE Trans. Geosci. Remote Sens.*, vol. 53, no. 5, pp. 2664–2682, 2014. doi: 10.1109/TGRS.2014.2363548.
- [130] K. Zhou, B. Gorte, R. Lindenbergh, and E. Widyaningrum, "3d building change detection between current VHR images and past lidar data," *Int. Arch. Photogramm. Remote Sens. Spatial Inf. Sci.*, vol. XLII-2, no. 2, pp. 1229–1235, 2018. doi: 10.5194/isprs-archives-XLII-2-1229-2018.
- [131] T. Bai, K. Sun, S. Deng, D. Li, W. Li, and Y. Chen, "Multi-scale hierarchical sampling change detection using random forest for high-resolution satellite imagery," *Int. J. Remote Sens.*, vol. 39, no. 21, pp. 7523–7546, 2018. doi: 10.1080/01431161.2018.1471542.
- [132] X. Zhang and S. Du, "Learning selfhood scales for urban land cover mapping with very-high-resolution satellite images," *Remote Sens. Environ.*, vol. 178, pp. 172–190, June 2016. doi: 10.1016/j.rse.2016.03.015.
- [133] D. Wen, X. Huang, L. Zhang, and J. A. Benediktsson, "A novel automatic change detection method for urban high-resolution remotely sensed imagery based on multiindex scene representation," *IEEE Trans. Geosci. Remote Sens.*, vol. 54, no. 1, pp. 609–625, 2015. doi: 10.1109/TGRS.2015.2463075.
- [134] S. Aleksandrowicz, K. Turlej, S. Lewiski, and Z. Bochenek, "Change detection algorithm for the production of land cover change maps over the European union countries," *Remote Sens.*, vol. 6, no. 7, pp. 5976–5994, 2014. doi: 10.3390/rs6075976.
- [135] G. Jianya, S. Haigang, M. Guorui, and Z. Qiming, "A review of multi-temporal remote sensing data change detection algorithms," *Int. Archives Photogrammetry, Remote Sens. Spatial Inform. Sci.*, vol. 37, no. B7, pp. 757–762, 2008.
- [136] L. Dong and J. Shan, "A comprehensive review of earthquake-induced building damage detection with remote sensing techniques," *ISPRS J. Photogrammetry Remote Sens.*, vol. 84, pp. 85–99, 2013. doi: 10.1016/j.isprsjprs.2013.06.011.
- [137] A. Hecheltjen, F. Thonfeld, and G. Menz, "Recent advances in remote sensing change detection-a review," in *Land Use and Land Cover Mapping in Europe*, I. Manakos and M. Braun, Eds. Dordrecht: Springer, 2014, pp. 145–178.
- [138] M. Li, S. Zang, B. Zhang, S. Li, and C. Wu, "A review of remote sensing image classification techniques: The role of spatio-contextual information," *Eur. J. Remote Sens.*, vol. 47, no. 1, pp. 389–411, 2014. doi: 10.5721/EuJRS20144723.
- [139] Z. Li, W. Shi, P. Lu, L. Yan, Q. Wang, and Z. Miao, "Landslide mapping from aerial photographs using change detection-based Markov random field," *Remote Sens. Environ.*, vol. 187, pp. 76–90, Dec. 2016. doi: 10.1016/j.rse.2016.10.008.
- [140] Y. Bazi, F. Melgani, and H. D. Al-Sharari, "Unsupervised change detection in multispectral remotely sensed imagery with level set methods," *IEEE Trans. Geosci. Remote Sens.*, vol. 48, no. 8, pp. 3178–3187, 2010. doi: 10.1109/TGRS.2010.2045506.
- [141] V. Neagoe, R. Stoica, A. Ciurea, L. Bruzzone, and F. Bovolo, "Concurrent self-organizing maps for supervised/unsupervised change detection in remote," *IEEE J. Sel. Topics Appl. Earth Observ. Remote Sens.*, vol. 7, no. 8, pp. 3525–3533, 2014. doi: 10.1109/JSTARS.2014.2330808.
- [142] L. Bruzzone and D. F. Prieto, "Automatic analysis of the difference image for unsupervised change detection," *IEEE Trans. Geosci. Remote Sens.*, vol. 38, no. 3, pp. 1171–1182, 2000. doi: 10.1109/36.843009.
- [143] T. Celik, "Unsupervised change detection in satellite images using principal component analysis and k-means clustering," *IEEE Geosci. Remote Sens. Lett.*, vol. 6, no. 4, pp. 772–776, 2009. doi: 10.1109/LGRS.2009.2025059.
- [144] S. Liu, L. Bruzzone, F. Bovolo, M. Zanetti, and P. Du, "Sequential spectral change vector analysis for iteratively discovering and detecting multiple changes in hyperspectral images," *IEEE Trans. Geosci. Remote Sens.*, vol. 53, no. 8, pp. 4363–4378, 2015. doi: 10.1109/TGRS.2015.2396686.
- [145] X. Zhang, W. Shi, P. Liang, and M. Hao, "Level set evolution with local uncertainty constraints for unsupervised change detection," *Remote Sens. Lett.*, vol. 8, no. 8, pp. 811–820, 2017. doi: 10.1080/2150704X.2017.1317929.
- [146] L. Wan, T. Zhang, and H. You, "Multi-sensor remote sensing image change detection based on sorted histograms," *Int. J. Remote Sens.*, vol. 39, no. 11, pp. 3753–3775, 2018. doi: 10.1080/01431161.2018.1448481.
- [147] Z. Lv, T. Liu, and J. A. Benediktsson, "Object-oriented key point vector distance for binary land cover change detection using VHR remote sensing images," *IEEE Trans. Geosci. Remote Sens.*, vol. 58, no. 9, pp. 6524–6533, 2020. doi: 10.1109/TGRS.2020.2977248.
- [148] G. Chen, G. J. Hay, L. M. Carvalho, and M. A. Wulder, "Object-based change detection," *Int. J. Remote Sens.*, vol. 33, no. 14, pp. 4434–4457, 2012. doi: 10.1080/01431161.2011.648285.
- [149] D. Lu, P. Mausel, E. Brondizio, and E. Moran, "Change detection techniques," *Int. J. Remote Sens.*, vol. 25, no. 12, pp. 2365–2401, 2004. doi: 10.1080/0143116031000139863.
- [150] W. Shi and M. Ehlers, "Determining uncertainties and their propagation in dynamic change detection based on classified remotely-sensed images," *Int. J. Remote Sens.*, vol. 17, no. 14, pp. 2729–2741, 1996. doi: 10.1080/01431169608949103.
- [151] T. Lei, Y. Zhang, Z. Lv, S. Li, S. Liu, and A. K. Nandi, "Landslide inventory mapping from bitemporal images using deep convolutional neural networks," *IEEE Geosci. Remote Sens. Lett.*, vol. 16, no. 6, pp. 982–986, 2019. doi: 10.1109/LGRS.2018.2889307.
- [152] Q. Wang, X. Zhang, G. Chen, F. Dai, Y. Gong, and K. Zhu, "Change detection based on faster r-CNN for high-resolution remote sensing images," *Remote Sens. Lett.*, vol. 9, no. 10, pp. 923–932, 2018. doi: 10.1080/2150704X.2018.1492172.